Sensor and Simulation Notes
Note 202

October 1973

Diffraction of the Pulsed Field from an Arbitrarily Oriented Electric or Magnetic Dipole by a Wedge

by

K.K. Chan, L.B. Felsen, S.T. Peng and J. Shmoys
Department of Electrical Engineering and Electrophysics
Polytechnic Institute of New York, Farmingdale, N.Y.

Abstract

A new closed form solution in terms of elementary functions is developed for the fields radiated by an impulsively excited electric or magnetic dipole oriented arbitrarily in the presence of a perfectly conducting wedge. Previously, this type of solution has been available only for dipoles oriented parallel to the edge. The solution for the required two-component Hertz vector is constructed by an image method utilizing an infinitely extended angular space, and expressions for the electromagnetic field components are derived therefrom. It is shown that the new result reduces properly to known solutions in the limiting cases where a) the wedge degenerates into a half plane and b) the source is moved to infinity to generate an incident plane pulse. For application to parallel plane waveguide simulators fed by a conical transmission line, it is of interest to examine temporal source functions that lead to local simulation of an incident step function plane wave field by transient dipoles. Such temporal source profiles are derived and are employed for numerical evaluation of the resulting diffracted field. The field plots are compared with those obtained previously for plane wave incidence and permit an assessment of the effect of source location.

I. Introduction

One type of parallel plane simulator for EMP diffraction involves a conical, two-conductor feed region that is joined to the parallel plane region by a bend in the conductors. Since the junction affects the incoming electromagnetic field, it is necessary to understand the effect of the bend on the field transmitted into the parallel plane test region. Because of the complexity of the actual junction problem, attention has been given to the simplest constituent configuration, an interior or exterior bend in a single, infinite, plane, perfectly conducting sheet. For large exterior bend angles, a sharp edge is produced and the resulting configuration, a wedge, is of interest for applications involving terminated ground planes. In previous studies in this series [1, 2], the incident electromagnetic field was assumed to be a plane pulse incident perpendicularly to the edge, along one face of the wedge. For applications involving parallel plane simulators or finite ground planes, a more realistic incident field is provided by a spherical pulse generated, for example, by an arbitrarily oriented electric or magnetic dipole source. The present note is concerned with the solution of dipole diffraction by a wedge.

The wedge diffraction problem is one of the first to have been treated by rigorous analysis. While the early concern was with the time-harmonic regime, the solution for which could be represented variously by integral transform and eigenfunction expansions, it was found subsequently that pulse diffraction results were sometimes obtainable in closed form. An excellent summary of the history of wedge diffraction may be found in the paper by Oberhettinger [3]. It is shown there that the scalar field solutions for plane and spherical delta function pulses incident on a wedge with Dirichlet or Neumann boundary conditions can be obtained in terms of elementary functions. Since the electromagnetic fields radiated by axial* electric and magnetic dipoles can be derived by differentiation from the scalar Dirichlet and Neumann solutions, respectively, it follows that these fields are also expressible in closed form. However, closed form results have not previously been presented

---

* The terms "axial" and "transverse" denote directions parallel and perpendicular, respectively, to the edge of the wedge.

for the non-scalarizable fields radiated by transverse dipoles. It is shown here that such solutions may indeed be developed, by a fundamental procedure utilizing an image representation in an infinitely extended angular space. Thus, a principal new result of the present study is the construction of a closed form solution of the time-dependent dyadic Green's function for a perfectly conducting wedge. For the special case when the wedge degenerates into a half plane, a closed form for the dyadic Green's function has recently been given [4]. It is shown that our wedge solution reduces properly to the half-plane limit. By moving the dipole source to infinity, one may generate near the edge an incident plane wave field. Our solution reduces to the known results also in that limit.

In establishing a connection with the previous numerical solutions of Baum [1] and Higgins [2], it is of interest to explore the deviation of the spherical pulse solutions from the idealized plane pulse solutions. We have therefore considered simultaneous excitation by electric and magnetic dipoles with a time dependence such that the incident field at a selected point on the edge is the same as for a unit step incident plane wave. Plots of numerical results for the field near the edge have been made for some of the parameters used in [1] and [2] so that direct assessment of the influence of the source point distance from the edge is possible.

II. Formulation of the Problem

1. Use of Hertz potentials

The transient fields due to vector source distributions with arbitrary space-time dependence may be derived by integration of space-time dyadic Green's functions, which provide the fields excited by arbitrarily oriented electric and magnetic dipole sources with impulsive time dependence. If $\hat{\underset{\sim}{G}}_e(\underset{\sim}{r}, \underset{\sim}{r}';t,t')$ and $\hat{\underset{\sim}{G}}_m(\underset{\sim}{r}, \underset{\sim}{r}';t,t')$ denote electric and magnetic dyadic Green's functions, respectively, then the vector electric field $\hat{\underset{\sim}{E}}_e(\underset{\sim}{r}, \underset{\sim}{r}';t,t')$ due to an impulsive electric dipole with moment density

$$\underset{\sim}{P}(\underset{\sim}{r}, t) = \underset{\sim}{p}(\underset{\sim}{r}')\delta(\underset{\sim}{r}-\underset{\sim}{r}')\,\delta(t-t') \tag{1}$$

is given by

$$\hat{\underset{\sim}{E}}_e(\underset{\sim}{r}, \underset{\sim}{r}';t,t') = - \hat{\underset{\sim}{G}}_e(\underset{\sim}{r}, \underset{\sim}{r}';t,t') \cdot \underset{\sim}{p}\ , \tag{2}$$

while the vector magnetic field $\hat{H}_m(\underset{\sim}{r}, \underset{\sim}{r}';t,t')$ due to an impulsive magnetic dipole with moment density

$$\underset{\sim}{M}(\underset{\sim}{r}, t) = \underset{\sim}{m}(\underset{\sim}{r}')\,\delta(\underset{\sim}{r}-\underset{\sim}{r}')\,\delta(t-t') \tag{3}$$

is given by

$$\hat{\underset{\sim}{H}}_m(\underset{\sim}{r}, \underset{\sim}{r}';t,t') = - \hat{\underset{\sim}{G}}_m(\underset{\sim}{r}, \underset{\sim}{r}';t,t') \cdot \underset{\sim}{m}\ . \tag{4}$$

Here, $\underset{\sim}{p}$ and $\underset{\sim}{m}$ are (generally non-coinciding) unit vectors at the source point $\underset{\sim}{r}'$. The magnetic field $\hat{\underset{\sim}{H}}_e$ corresponding to $\hat{\underset{\sim}{E}}_e$ in (2) and the electric field $\hat{\underset{\sim}{E}}_m$ corresponding to $\hat{\underset{\sim}{H}}_m$ in (4) are then obtained from the time-dependent Maxwell field equations. According to causality, all fields vanish identically for $t < t'$.

In the present treatment, it will be more convenient to deal directly with the fields $\hat{\underset{\sim}{E}}$ and $\hat{\underset{\sim}{H}}$ instead of the dyadic Green's functions. Calculation of the former is simplified through use of the electric and magnetic Hertz vectors $\hat{\underset{\sim}{\Pi}}_e(\underset{\sim}{r}, \underset{\sim}{r}';t,t')$ and $\hat{\underset{\sim}{\Pi}}_m(\underset{\sim}{r}, \underset{\sim}{r}';t,t')$, respectively, which are solutions of the time-dependent wave equations

$$\left(\nabla^2 - \mu\epsilon\frac{\partial^2}{\partial t^2}\right)\hat{\underset{\sim}{\Pi}}_e(\underset{\sim}{r}, \underset{\sim}{r}';t,t') = - \frac{1}{\epsilon}\,\underset{\sim}{P}(\underset{\sim}{r}, t)\ , \tag{5}$$

$$\left(\nabla^2 - \mu\epsilon\frac{\partial^2}{\partial t^2}\right)\hat{\underset{\sim}{\Pi}}_m(\underset{\sim}{r}, \underset{\sim}{r}';t,t') = - \underset{\sim}{M}(\underset{\sim}{r}, t)\ . \tag{6}$$

Then [5]

$$\hat{\underset{\sim}{E}}_e(\underset{\sim}{r}, \underset{\sim}{r}'; t, t') = \nabla\nabla \cdot \hat{\underset{\sim}{\Pi}}_e(\underset{\sim}{r}, \underset{\sim}{r}'; t, t') - \mu\epsilon \frac{\partial^2}{\partial t^2} \hat{\underset{\sim}{\Pi}}_e(\underset{\sim}{r}, \underset{\sim}{r}'; t, t') \tag{7}$$

$$\hat{\underset{\sim}{H}}_e(\underset{\sim}{r}, \underset{\sim}{r}'; t, t') = \epsilon \nabla \times \frac{\partial}{\partial t} \hat{\underset{\sim}{\Pi}}_e(\underset{\sim}{r}, \underset{\sim}{r}'; t, t'), \tag{8}$$

and

$$\hat{\underset{\sim}{H}}_m(\underset{\sim}{r}, \underset{\sim}{r}'; t, t') = \nabla\nabla \cdot \hat{\underset{\sim}{\Pi}}_m(\underset{\sim}{r}, \underset{\sim}{r}'; t, t') - \mu\epsilon \frac{\partial^2}{\partial t^2} \hat{\underset{\sim}{\Pi}}_m(\underset{\sim}{r}, \underset{\sim}{r}'; t, t') \ , \tag{9}$$

$$\hat{\underset{\sim}{E}}_m(\underset{\sim}{r}, \underset{\sim}{r}'; t, t') = -\mu \nabla \times \frac{\partial}{\partial t} \hat{\underset{\sim}{\Pi}}_m(\underset{\sim}{r}, \underset{\sim}{r}'; t, t') \ , \tag{10}$$

with ϵ and μ representing the (dispersionless) permittivity and permeability in the homogeneous medium.

If the electric and magnetic dipole moments are distributed throughout a volume V with density functions $f_e(\underset{\sim}{r})$ and $f_m(\underset{\sim}{r})$, respectively, then the corresponding electromagnetic fields are

$$\check{\underset{\sim}{E}}_i(\underset{\sim}{r}; t, t') = \int_V f_i(\underset{\sim}{r}') \hat{\underset{\sim}{E}}_i(\underset{\sim}{r}, \underset{\sim}{r}'; t, t') \, d\underset{\sim}{r}' \ , \quad i=e \text{ or } m, \tag{11}$$

and similarly for $\check{\underset{\sim}{H}}_i$. Note that the orientation of $\underset{\sim}{p}(\underset{\sim}{r}')$ and $\underset{\sim}{m}(\underset{\sim}{r}')$ may change with $\underset{\sim}{r}'$. Alternatively, if the electric and magnetic dipole moments have the respective temporal variations $F_e(t)$ and $F_m(t)$ for $t > 0$, with $F_{e,m} \equiv 0$ for $t < 0$, then the corresponding electromagnetic fields are

$$\overline{\underset{\sim}{E}}_i(\underset{\sim}{r}, \underset{\sim}{r}', t) = \int_0^t F_i(t') \hat{\underset{\sim}{E}}_i(\underset{\sim}{r}, \underset{\sim}{r}'; t, t') dt', \quad i=e \text{ or } m, \tag{12}$$

and similarly for $\overline{\underset{\sim}{H}}_i$. Finally, if the dipole moments are spatially distributed and are active over a specified time interval, the corresponding fields are obtained on integration of $\hat{\underset{\sim}{E}}_i$ and $\hat{\underset{\sim}{H}}_i$ over the appropriate space-time volume.

2. Boundary conditions for a perfectly conducting wedge

When the dipole sources in (1) and (3) are located in the presence of a perfectly conducting wedge, the tangential electric field on the wedge must vanish, and an "edge condition" must be satisfied, for all t. If the wedge faces are located on the half planes $\phi = 0$ and $\phi = \alpha$ in a cylindrical (ρ, ϕ, z)

coordinate system (see Fig. 1), then the required conditions are $E_\rho = E_z = 0$ at $\phi = 0, \alpha$. Expanding the right hand side of (7) into cylindrical components, one may show that the boundary conditions are satisfied if

$$\hat{\Pi}_{e\rho} = 0, \quad \frac{\partial}{\partial\phi}\hat{\Pi}_{e\phi} = 0, \quad \hat{\Pi}_{ez} = 0, \quad \text{at } \phi = 0, \alpha \ . \tag{13}$$

Similarily, it follows from (10) that the magnetic potential must satisfy

$$\frac{\partial}{\partial\phi}\hat{\Pi}_{m\rho} = 0, \quad \hat{\Pi}_{m\phi} = 0, \quad \frac{\partial}{\partial\phi}\hat{\Pi}_{mz} = 0, \quad \text{at } \phi = 0, \alpha \ . \tag{14}$$

It will be convenient to represent the Hertz vectors in rectangular rather than cylindrical component form. Since

$$\hat{\Pi}_\rho = \hat{\Pi}_x \cos\phi + \hat{\Pi}_y \sin\phi, \quad \hat{\Pi}_\phi = -\hat{\Pi}_x \sin\phi + \hat{\Pi}_y \cos\phi \ , \tag{15}$$

one may write (13) and (14) as

$$\hat{\Pi}_{ex}\cos\phi + \hat{\Pi}_{ey}\sin\phi = 0, \quad \frac{\partial}{\partial\phi}\left[-\hat{\Pi}_{ex}\sin\phi + \hat{\Pi}_{ey}\cos\phi\right] = 0, \quad \hat{\Pi}_{ez} = 0, \tag{16}$$

$$\frac{\partial}{\partial\phi}\left[\hat{\Pi}_{mx}\cos\phi + \hat{\Pi}_{my}\sin\phi\right] = 0, \quad -\hat{\Pi}_{mx}\sin\phi + \hat{\Pi}_{my}\cos\phi = 0, \quad \frac{\partial}{\partial\phi}\hat{\Pi}_{mz} = 0, \tag{17}$$

at $\phi = 0$ and $\phi = \alpha$. These rectangular components then satisfy the wave equations [see (1), (3), (5) and (6)]:

$$\left(\nabla^2 - \mu\epsilon\frac{\partial^2}{\partial t^2}\right)\hat{\Pi}_{\substack{ex \\ mx}} = -\left\{\begin{array}{c} \frac{1}{\epsilon}\cos\nu_e\cos\theta_e \\ \\ \cos\nu_m\cos\theta_m \end{array}\right\}\delta(\underset{\sim}{r}-\underset{\sim}{r}')\,\delta(t-t') \ , \tag{18}$$

$$\left(\nabla^2 - \mu\epsilon\frac{\partial^2}{\partial t^2}\right)\hat{\Pi}_{\substack{ey \\ my}} = -\left\{\begin{array}{c} \frac{1}{\epsilon}\sin\nu_e\cos\theta_e \\ \\ \sin\nu_m\cos\theta_m \end{array}\right\}\delta(\underset{\sim}{r}-\underset{\sim}{r}')\,\delta(t-t') \ , \tag{19}$$

$$\left(\nabla^2 - \mu\epsilon\frac{\partial^2}{\partial t^2}\right)\hat{\Pi}_{\substack{ez \\ mz}} = -\left\{\begin{array}{c} \frac{1}{\epsilon}\sin\theta_e \\ \\ \sin\theta_m \end{array}\right\}\delta(r-r')\,\delta(t-t') \ , \tag{20}$$

where ν_i and θ_i, with i=e, m, determine the dipole orientation at $\underset{\sim}{r}'$:

$$\underset{\sim}{p} = \underset{\sim}{x}_o \cos \nu_e \cos \theta_e + \underset{\sim}{y}_o \sin \nu_e \cos \theta_e + \underset{\sim}{z}_o \sin \theta_e,$$
$$\underset{\sim}{m} = \underset{\sim}{x}_o \cos \nu_m \cos \theta_m + \underset{\sim}{y}_o \sin \nu_m \cos \theta_m + \underset{\sim}{z}_o \sin \theta_m. \tag{21}$$

ν_e and ν_m are the orientation angles of the projections of the electric and magnetic dipoles, respectively, on the x-y plane, while θ_e and θ_m are the angles of inclination of the dipoles with the x-y plane; $\nu_{e,m}$ is measured counterclockwise from the positive x-axis. When θ_e and θ_m equals $\pi/2$ (z-directed dipole), the electromagnetic field is derivable solely from the single component $\hat{\Pi}_{ez}$ or $\hat{\Pi}_{mz}$ of the Hertz potential. When θ_e or θ_m equals zero (transverse dipole), one requires the two transverse components $\hat{\Pi}_{e\,x,y}$ or $\hat{\Pi}_{m\,x,y}$, which are coupled by the boundary conditions.

The preceding formulation has previously been presented for time-harmonic problems [6], and its extension to the time-dependent case has been straightforward.

III. Relation Between a Class of Time-Harmonic and Time-Dependent Problems

For some diffraction problems, the time-dependent solution turns out to be simpler in form than the time-harmonic solution. In particular, it has been noted [7] that for certain integral representations of the time-harmonic field, there exists a direct inversion yielding a closed form for the transient field. If a time-harmonic scalar Green's function $G(\underset{\sim}{r}, \underset{\sim}{r}'; w)$ (i.e., the time-harmonic response to point source excitation at $\underset{\sim}{r}'$) can be expressed as a Sommerfeld integral

$$G(\underset{\sim}{r}, \underset{\sim}{r}'; w) = \int_C \xi(\underset{\sim}{r}, \underset{\sim}{r}', w) \exp\left[i \frac{w}{c} \gamma(\underset{\sim}{r}, \underset{\sim}{r}', w) \right] dw \tag{22}$$

where C is the integration path in Fig. 2 (symmetrical about w=0), w is the frequency, $c=(\mu \epsilon)^{-\frac{1}{2}}$ is the speed of light, and an $\exp(-iwt)$ dependence is suppressed, then the time-dependent scalar Green's function $\hat{G}(\underset{\sim}{r}, \underset{\sim}{r}';t,t')$ corresponding to excitation by a point source at $\underset{\sim}{r}'$ with impulsive behavior $\delta(t-t')$ is given by:

$$\hat{G}(\underset{\sim}{r}, \underset{\sim}{r}':t,t') = 0, \quad t-t' < \frac{R}{c}, \quad R = \gamma(r, r', 0) \tag{23a}$$

$$= -2c \frac{\mathrm{Re}[i \xi(\underset{\sim}{r}, \underset{\sim}{r}', -i\beta)]}{(d/d\beta)\, \gamma(\underset{\sim}{r}, \underset{\sim}{r}', -i\beta)}, \quad t-t' > \frac{R}{c} \tag{23b}$$

Here, $\beta = \beta(\underset{\sim}{r}, \underset{\sim}{r}', t-t')$ is defined implicitly by

$$c(t-t') = \gamma(\underset{\sim}{r}, \underset{\sim}{r}' - i\beta), \tag{24}$$

and it has been assumed that $i\xi(\underset{\sim}{r}, \underset{\sim}{r}', w)$ is real for real w, and that $\gamma(\underset{\sim}{r}, \underset{\sim}{r}', -i\beta)$ is real for real β.

It has been shown previously [7] that the scalar time-harmonic Green's functions for a wedge with Dirichlet (G=0) and Neumann ($\partial G/\partial \phi = 0$) type boundary conditions can be expressed in the form (22) whence the corresponding time-dependent Green's functions are given explicitly by (23). It may be noted from (16) and from (18) - (20) that for a z-directed electric dipole, which generates a Hertz vector $\hat{\underset{\sim}{\Pi}}_e = \underset{\sim}{z}_o \hat{\Pi}_{ez}$, the scalar function $\epsilon \Pi_{ez}$ is equal to the Green's function with Dirichlet boundary conditions. Similarly, from (17) and from (18) - (20), a z-directed magnetic dipole generates a Hertz vector

$\hat{\underset{\sim}{\Pi}}_m = \underset{\sim}{z}_o \hat{\Pi}_{mz}$, with the scalar function Π_{mz} equal to the Green's function satisisfying the Neumann boundary conditions. When the dipoles are not oriented parallel to the edge of the wedge (z-axis), the required transverse components of the Hertz vector are not directly expressible in terms of scalar Green's functions, as is evident from (16) - (19). Nevertheless, it is found to be possible to express Π_{ix} and Π_{iy}, i = e or m, in the form of an integral as in (22) and thus to provide the transient solutions $\hat{\Pi}_{ix}$ and $\hat{\Pi}_{iy}$ in the elementary form (23). Moreover, one may relate $\hat{\Pi}_{ix}$ and $\hat{\Pi}_{iy}$ to the scalar Neumann and Dirichlet Green's functions, but not in a simple fashion. These aspects are considered subsequently.

IV. Construction of the Solution by Image Method

Since the perfectly conducting wedge is a "separable" boundary surface in a cylindrical or spherical coordinate system, the method of separation of variables can be employed to construct a variety of alternative representations of the field solution. Such representations have been discussed in [7], and the choice of a particular representation depends on the parameter range under consideration. For construction of the transient solution in closed form, an image representation in an infinitely extended angular space [7] is highly suitable since the time-harmonic field generated by a typical scalar source in such a space is expressible in the form (22): the corresponding transient field is therefore given simply as in (23). Moreover, it has been found that the scalar images can be summed into a closed form. This has led to the known result, in terms of elementary functions, for the transient field generated when an incident scalar spherical pulse is diffracted by a wedge [3]. In view of the remarks made previously, these scalar solutions may be employed directly for calculation of the field due to a pulsed electric or magnetic dipole directed parallel to the z-axis.

For transversely oriented pulsed dipoles, a closed form solution in terms of elementary functions has not been reported previously when the wedge angle α is arbitrary; for the special case of a thin half plane ($\alpha = 2\pi$), such a solution has been published recently [4]. We shall demonstrate below that the image method is successful in dealing with the vector problem and in providing a closed form result for arbitrary wedge angles.

1. Time-harmonic solution

An arbitrarily oriented electric or magnetic dipole may be regarded as a superposition of longitudinal and transverse dipoles. For convenience, we list first the known result for the longitudinal case; we then construct the solution for the transverse case. A time dependence $\exp(-i\omega t)$ is suppressed throughout. Equations (16) - (21) apply to the time-harmonic problem provided that $\partial^2/\partial t^2 \rightarrow -\omega^2$ and the $\delta(t-t')$ factor is omitted.

a) longitudinal dipoles

The electromagnetic fields due to a longitudinal electric dipole of unit moment strength (i.e., $\underset{\sim}{p}=\underset{\sim}{z}_o$) may be derived from the z-component of the electric Hertz potential, $\Pi_{ez}(\underset{\sim}{r}, \underset{\sim}{r}', \omega)$. This potential may be separated into a geometric optical part, Π^g_{ez}, and a diffracted part, Π^d_{ez} :

$$\Pi_{ez} = \Pi^{g}_{ez} + \Pi^{d}_{ez} \quad . \tag{25}$$

The geometric - optical part accounts for rays that emanate from the source and are multiply reflected between the wedge faces:

$$\Pi^{g}_{ez}(\underset{\sim}{r}, \underset{\sim}{r}', \omega) = \frac{1}{\epsilon}\sum_{n} \frac{\exp\left[ik\left|\underset{\sim}{r}-\underset{\sim}{r}_{n}\right|\right]}{4\pi\left|\underset{\sim}{r}-\underset{\sim}{r}_{n}\right|} U(\pi - |\phi - \phi_{n}|)$$

$$- \frac{1}{\epsilon}\sum_{n} \frac{\exp\left[ik\left|\underset{\sim}{r}-\overline{\underset{\sim}{r}}_{n}\right|\right]}{4\pi\left|\underset{\sim}{r}-\overline{\underset{\sim}{r}}_{n}\right|} U(\pi - |\phi - \overline{\phi}_{n}|) \quad , \tag{26}$$

where $k = \omega/c$, and $U(a) = 1$ or 0 for $a > 0$ and $a < 0$, respectively, while

$$\phi_{n} = 2n\alpha + \phi', \quad \overline{\phi}_{n} = 2n\alpha - \phi', \quad n = 0, \pm 1, \pm 2 \ldots \tag{27}$$

$$\underset{\sim}{r}_{n} = (\rho', \phi_{n}, z'), \quad \overline{\underset{\sim}{r}}_{n} = (\rho', \overline{\phi}_{n}, z'), \quad \underset{\sim}{r}_{o} \equiv \underset{\sim}{r}' = (\rho', \phi', z') \, . \tag{28}$$

The diffracted part, which accounts for radiation scattered by the edge, may be written in the form of the integral (22), with

$$\gamma(\underset{\sim}{r}, \underset{\sim}{r}', w) = \left[\rho^2 + \rho'^2 + (z-z')^2 + 2\rho\rho' \cos w\right]^{\frac{1}{2}} \tag{29}$$

$$F(\underset{\sim}{r}, \underset{\sim}{r}', w) = -\frac{i}{8\pi^2\epsilon} \frac{B(\phi,\phi'; w) - B(\phi,-\phi'; w)}{\gamma(\underset{\sim}{r}, \underset{\sim}{r}'; w)} \tag{30}$$

$$B(\phi, \phi'; w) = \frac{\pi}{\alpha} \sin\frac{\pi^2}{\alpha} \frac{1}{\cos\left[\frac{\pi}{\alpha}(w - \phi + \phi')\right] - \cos\frac{\pi^2}{\alpha}} \quad ,$$

where $\mathrm{Im}\ \nu > 0$ on c.

Similarly, the electromagnetic fields due to a longitudinal magnetic dipole of unit moment strength (i.e., $\underset{\sim}{m} = \underset{\sim}{z}_{o}$) may be derived from the z-component of the magnetic Hertz potential, $\Pi_{em}(\underset{\sim}{r}, \underset{\sim}{r}', \omega)$:

$$\Pi_{em} = \Pi^{g}_{em} + \Pi^{d}_{em} \, , \tag{31}$$

where the geometric optical part is given by

$$\Pi^{g}_{em}(r, r', \omega) = \sum_{n} \frac{\exp[ik|\underset{\sim}{r}-\underset{\sim}{r}_n|]}{4\pi|\underset{\sim}{r}-\underset{\sim}{r}_n|} U(\pi - |\phi - \phi_n|)$$

$$+ \sum_{n} \frac{\exp[ik|\underset{\sim}{r}-\bar{\underset{\sim}{r}}_n|]}{4\pi|\underset{\sim}{r}-\bar{\underset{\sim}{r}}_n|} U(\pi - |\phi - \bar{\phi}_n|) . \qquad (32)$$

The diffracted part may be written in the form of the integral (22), with

$$\xi(\underset{\sim}{r}, \underset{\sim}{r}', w) = -\frac{i}{8\pi^2} \frac{B(\phi, \phi'; w) + B(\phi, -\phi'; w)}{\gamma(\underset{\sim}{r}, \underset{\sim}{r}'; w)} \qquad (33)$$

and $\gamma(\underset{\sim}{r}, \underset{\sim}{r}'; w)$ given by (29).

The preceding results for Π_{ez} and Π_{mz} are exact; they are especially useful for the high-frequency range, or for large distances (in terms of wavelength) of the source and observation points from the edge, since the diffraction integrals can then be reduced by asymptotic techniques.

b) transverse dipoles

When the dipoles are transverse to z ($\theta_{e,m} = 0$ in (21)), the electromagnetic fields are derivable from $\Pi_{i\,x,y}$, $i = e$ or m. To synthesize these Hertz potentials in the form of (22), with ξ given in a closed form, we utilize the same image procedure as for the longitudinal dipoles (see [7]). When $\alpha = \pi/N$, N integer, the effect of the wedge boundaries can be accounted for by a set of $(2N-1)$ image sources with appropriate orientation (Fig. 3). For arbitrary α, the image procedure may also be utilized; however, the set of images does not now close upon itself, and utilization of an infinitely extended ϕ-space is required. The source and images lie in the plane $z=z'$ on the circle $\rho=\rho'$ and decompose into two sets with the angular coordinates ϕ_n and $\bar{\phi}_n$ given in (27). An image at ϕ_n has the orientation

$$\underset{\sim}{p}_n = \underset{\sim}{x}_o \cos(2n\alpha + \nu_e) + \underset{\sim}{y}_o \sin(2n\alpha + \nu_e) , \qquad (34a)$$

while an image at $\bar{\phi}_n$ has the orientation

$$\bar{\underset{\sim}{p}}_n = -\underset{\sim}{x}_o \cos(2n\alpha - \nu_e) - \underset{\sim}{y}_o \sin(2n\alpha - \nu_e) . \qquad (34b)$$

The Hertz potentials $\Pi^{\infty}_{ex,y}$ excited by a typical image source in the infinitely extended angular space satisfy the time-harmonic form of (18) and (19) with

cos ν_e and sin ν_e replaced by the appropriate quantities from (34a) and (34b). Instead of (16), the boundary condition requires "outgoing waves" toward $\phi = \pm \infty$. The desired field solution in the wedge region follows on summation over all images.

To synthesize the solution for $\Pi^{\infty}_{ex,\,y}$ we consider first the time-harmonic, outgoing-wave, scalar Green's function $G^{\infty}(\underset{\sim}{r}, \underset{\sim}{r}', \omega)$ in the domain $-\infty < (\phi, \phi_o) < \infty$, $0 < (\rho, \rho') < \infty$, $-\infty < z < \infty$; this Green's function is defined by the equation:

$$(\nabla^2 + k^2)\, G^{\infty}(\underset{\sim}{r}, \underset{\sim}{r}_o, \omega) = -\delta(\underset{\sim}{r} - \underset{\sim}{r}_o), \quad \underset{\sim}{r}_o = (\rho', \phi_o, 0). \tag{35}$$

It is known that G^{∞} is representable as follows [7]:

$$G^{\infty}(r, r_o, \omega) = \frac{e^{ik|\underset{\sim}{r} - \underset{\sim}{r}_o|}}{4\pi|\underset{\sim}{r} - \underset{\sim}{r}_o|}\, U(\pi - |\phi - \phi_o|)$$

$$- \frac{i}{8\pi^2} \int_C \frac{\exp[ik\gamma(\underset{\sim}{r}, \underset{\sim}{r}_o, w)]}{\gamma(\underset{\sim}{r}, \underset{\sim}{r}_o, w)}\, A^{\infty}(\phi, \phi_o, w)\, dw, \tag{36}$$

where C is the integration path in Fig. 2, γ is defined in (29), and

$$|\underset{\sim}{r} - \underset{\sim}{r}_o| = \left[|\underset{\sim}{\rho} - \underset{\sim}{\rho}_o|^2 + z^2\right]^{\frac{1}{2}}, \tag{37}$$

$$A^{\infty}(\phi, \phi_o, w) = \frac{1}{\pi - |\phi - \phi_o| - w} + \frac{1}{\pi + |\phi - \phi_o| + w}. \tag{38}$$

Evidently, the form of (36) is the same as (22) whence recovery of the transient solution is immediate via (23). The source coordinate ϕ_o may stand for ϕ_n or $\overline{\phi}_n$. The first term in (36) represents the incident spherical wave in the geometrically illuminated region while the second term represents the diffraction field. Since the infinite angular space simulates boundary conditions on the face of a "perfectly absorbing" wedge, there are no geometrically reflected contributions. Comparing the time-harmonic form of (18) and (19) with (35) and replacing $\underset{\sim}{p}$ in (21), with $\theta_e = 0$, by $\underset{\sim}{p}_n$ in (34a) or $\overline{\underset{\sim}{p}}_n$ in (34b), it follows that the time-harmonic Hertz potential descriptive of a transverse vector dipole source at $\underset{\sim}{r}_o$ in an infinite angular space can be represented as:

$$\Pi^{\infty}_{ex}(\underset{\sim}{r}, \underset{\sim}{r}_n, \omega) = \frac{1}{\epsilon} \cos\,(2n\alpha + \nu_e)\, G^{\infty}(\underset{\sim}{r}, \underset{\sim}{r}_n, \omega)\ , \tag{39a}$$

$$\Pi^{\infty}_{ey}(\underset{\sim}{r}, \underset{\sim}{r}_n, \omega) = \frac{1}{\epsilon} \sin\,(2n\alpha + \nu_e)\, G^{\infty}(\underset{\sim}{r}, \underset{\sim}{r}_n, \omega)\ , \tag{39b}$$

$$\Pi^{\infty}_{ex}(\underset{\sim}{r}, \overline{\underset{\sim}{r}}_n, \omega) = -\frac{1}{\epsilon} \cos\,(2n\alpha - \nu_e)\, G^{\infty}(\underset{\sim}{r}, \overline{\underset{\sim}{r}}_n, \omega)\ , \tag{40a}$$

$$\Pi^{\infty}_{ey}(\underset{\sim}{r}, \overline{\underset{\sim}{r}}_n, \omega) = -\frac{1}{\epsilon} \sin\,(2n\alpha - \nu_e)\, G^{\infty}(\underset{\sim}{r}, \overline{\underset{\sim}{r}}_n, \omega)\ . \tag{40b}$$

To synthesize the Hertz potentials for the perfectly conducting wedge, the solutions in (39) and (40) must be summed over all n. The contributions from the first term in (36) will be finite in number and yield the geometrically reflected fields. However, all of the images contribute to the diffracted field as represented by the second term in (36). Since ϕ_o occurs only in A^{∞}, the images may be grouped so as to be included in one or the other of the following summable series [8]:*

$$\sum_{n=-\infty}^{\infty} \frac{\cos 2n\alpha}{n-\psi} = -\pi\, \frac{\cos\,(2\alpha - \pi)\psi}{\sin \pi\psi}\ , \tag{41a}$$

$$\sum_{n=-\infty}^{\infty} \frac{\sin 2n\alpha}{n-\psi} = -\pi\, \frac{\sin\,(2\alpha - \pi)\psi}{\sin \pi\psi}\ , \tag{41b}$$

where ψ has the form $(2\alpha)^{-1}\,[\phi \mp \phi' \mp (\pi+w)]$, with all combinations of signs occurring. In achieving the grouping of images, and also for simplification of the result, one may utilize the fact that γ in (29) is an even function of w and that the integration path C in (36) is symmetrical with respect to w=0; thus, only those portions of the image sums that are even functions of w contribute to the integral. Details are given in Appendix A.

Performing these manipulations yields the following solution for the time-harmonic Hertz vector:

$$\underset{\sim}{\Pi}_e(\underset{\sim}{r}, \underset{\sim}{r}', \omega) = \underset{\sim}{\Pi}^{g}_e(\underset{\sim}{r}, \underset{\sim}{r}', \omega) + \underset{\sim}{\Pi}^{d}_e(\underset{\sim}{r}, \underset{\sim}{r}', \omega),\ \underset{\sim}{r}' = (\rho', \phi', z')\ , \tag{42}$$

where $\underset{\sim}{\Pi}^{g}_e$ is the geometric-optical part

*While α has to be restricted initially for applicability of (41a) and (41b), the closed form result can subsequently be employed for $0 < \alpha \leq 2\pi$.

$$\Pi^{g}_{e}(\underset{\sim}{r}, \underset{\sim}{r}', \omega) = \frac{1}{\epsilon}\sum_{n} \underset{\sim}{p}_{n} \frac{\exp[ik|\underset{\sim}{r} - \underset{\sim}{r}_{n}|]}{4\pi|\underset{\sim}{r} - \underset{\sim}{r}_{n}|} U(\pi - |\phi - \phi_{n}|)$$

$$+ \frac{1}{\epsilon}\sum_{n} \underset{\sim}{\bar{p}}_{n} \frac{\exp[ik|\underset{\sim}{r} - \underset{\sim}{\bar{r}}_{n}|]}{4\pi|\underset{\sim}{r} - \underset{\sim}{\bar{r}}_{n}|} U(\pi - |\phi - \bar{\phi}_{n}|) . \qquad (43)$$

The diffracted part $\underset{\sim}{\Pi}^{d}_{e}$ is given by

$$\Pi^{d}_{ex,\,y}(\underset{\sim}{r}, \underset{\sim}{r}', \omega) = -\frac{i}{8\pi^{2}\epsilon}\int_{C} \frac{\exp[ik\gamma(\underset{\sim}{r}, \underset{\sim}{r}', w)]}{\gamma(\underset{\sim}{r}, \underset{\sim}{r}', w)} A_{x,\,y}(\phi, \phi', w)dw, \qquad (44)$$

where

$$A_{x} = -\frac{\pi}{2\alpha}\left\{[Q_{1}(\phi-\phi') - Q_{1}(\phi+\phi')]\cos\nu - [Q_{2}(\phi-\phi') + Q_{2}(\phi+\phi')]\sin\nu\right\}, \qquad (45a)$$

$$A_{y} = -\frac{\pi}{2\alpha}\left\{[Q_{2}(\phi-\phi') - Q_{2}(\phi+\phi')]\cos\nu + [Q_{1}(\phi-\phi') + Q_{1}(\phi+\phi')]\sin\nu\right\}, \qquad (45b)$$

and

$$Q_{1}(\varphi) \equiv Q_{1}(\varphi, w) = \cos(\varphi-w-\pi)\cot\frac{\varphi-w-\pi}{2\alpha/\pi} - \cos(\varphi+w+\pi)\cot\frac{\varphi+w+\pi}{2\alpha/\pi}, \qquad (46a)$$

$$Q_{2}(\varphi) \equiv Q_{2}(\varphi, w) = \sin(\varphi-w-\pi)\cot\frac{\varphi-w-\pi}{2\alpha/\pi} - \sin(\varphi+w+\pi)\cot\frac{\varphi+w+\pi}{2\alpha/\pi}. \qquad (46b)$$

One may verify that $A_{x,\,y}$ and hence $\Pi^{d}_{ex,\,y}$ satisfy the boundary conditions (16). The form of the solution above is similar to that obtained by Malyuzhinets and Tuzhilin [6], who used a different procedure and different contours of integration for constructing the functions $A_{x,\,y}$.

For a magnetic dipole source transverse to z the image dipoles at ϕ_{n} are the same as $\underset{\sim}{p}_{n}$ in (34a) while those at $\bar{\phi}_{n}$ are given by $-\underset{\sim}{\bar{p}}_{n}$ in (34b). The solution for the magnetic Hertz vector therefore takes the same form as $\epsilon\underset{\sim}{\Pi}_{e}$ in (43) and (44) provided that the second sum in (43) and $Q_{1,\,2}(\phi+\phi')$ in (45) are multiplied by (-1), and that appropriate duality replacements are made when calculating the fields.

2. Transient solution

The time-dependent Hertz vector for a dipole with impulsive dipole moment is recovered at once on applying (22) and (23) to (25) - (30) for the longitudinal electric dipole, to (31) - (33) for the longitudinal magnetic dipole, to (42)-(46) for the transverse electric dipole, and to the above-noted modified version of (42)-(46) for the transverse magnetic dipole. The electromagnetic fields are then calculated from (7) - (10). The resulting expressions are listed below.

Longitudinal electric dipole

$$\hat{\Pi}_{ez} = \hat{\Pi}^{g}_{ez} + \hat{\Pi}^{d}_{ez} \tag{47}$$

$$\hat{\Pi}^{g}_{ez} = \frac{1}{\epsilon}\sum_{n} \frac{\delta(t-t' - |\underset{\sim}{r}-\underset{\sim}{r}_n|/c)}{4\pi|\underset{\sim}{r}-\underset{\sim}{r}_n|}\, U(\pi - |\phi-\phi_n|)$$

$$- \frac{1}{\epsilon}\sum_{n} \frac{\delta(t-t' - |\underset{\sim}{r}-\underset{\sim}{\bar{r}}_n|/c)}{4\pi|\underset{\sim}{r}-\underset{\sim}{\bar{r}}_n|}\, U(\pi - |\phi-\bar{\phi}_n|) \tag{47a}$$

$$\hat{\Pi}^{d}_{ez} = \frac{1}{\epsilon}\hat{G}^{d}_{1} = \frac{-c}{4\pi^2\epsilon} \frac{\text{Re } B(\phi, \phi';-i\beta) - \text{Re } B(\phi, -\phi';-i\beta)}{\rho\rho' \sinh\beta}\, U(t-t' - \frac{\ell}{c}) \tag{47b}$$

where $\hat{G}^{d}_{1}$ is the diffracted part of the scalar Dirichlet Green's function [7] and

$$\text{Re } B(\phi, \phi';-i\beta) = -\frac{\pi}{2\alpha}\left[\frac{\sin\frac{\pi}{\alpha}(\phi-\phi'-\pi)}{\cosh\frac{\pi\beta}{\alpha} - \cos\frac{\pi}{\alpha}(\phi-\phi'-\pi)} - \frac{\sin\frac{\pi}{\alpha}(\phi-\phi'+\pi)}{\cosh\frac{\pi\beta}{\alpha} - \cos\frac{\pi}{\alpha}(\phi-\phi'+\pi)}\right]$$

$$= -\frac{\pi}{2\alpha}\left[\sin\frac{\pi}{\alpha}(\phi-\phi'-\pi)\, A_{+} - \sin\frac{\pi}{\alpha}(\phi-\phi'+\pi)\, A_{-}\right], \tag{47c}$$

$$\cosh\beta = \frac{c^2(t-t')^2 - \rho^2 - \rho'^2 - (z-z')^2}{2\rho\rho'}, \quad \ell = \left[(\rho+\rho')^2 + (z-z')^2\right]^{\frac{1}{2}}. \tag{47d}$$

$$\hat{E}^g_{e\rho} = \frac{\partial^2}{\partial\rho\partial z}\hat{\Pi}^g_{ez}$$

$$= \frac{z-z'}{4\pi\epsilon}\sum_n \left[\rho-\rho'\cos(\phi-\phi_n)\right]\left[\frac{3}{r_n^5}\delta(t-t'-\frac{r_n}{c})+\frac{3}{cr_n^4}\delta'(t-t'-\frac{r_n}{c})+\frac{1}{c^2r_n^3}\delta''(t-t'-\frac{r_n}{c})\right]U(\pi-|\phi-\phi_n|)$$

$$-\frac{z-z'}{4\pi\epsilon}\sum_n \left[\rho-\rho'\cos(\phi-\overline{\phi}_n)\right]\left[\frac{3}{\overline{r}_n^5}\delta(t-t'-\frac{\overline{r}_n}{c})+\frac{3}{c\overline{r}_n^4}\delta'(t-t'-\frac{\overline{r}_n}{c})+\frac{1}{c^2\overline{r}_n^3}\delta''(t-t'-\frac{\overline{r}_n}{c})\right]U(\pi-|\phi-\overline{\phi}_n|) \tag{48a}$$

$$\hat{E}^d_{e\rho} = \frac{\partial^2}{\partial\rho\partial z}\hat{\Pi}^d_{ez} = J_1 - J_2\ , \tag{48b}$$

$$J_1 = \frac{K}{c^2}\frac{(z-z')(\rho+\rho')}{\ell^2\rho\rho'}\operatorname{csch}\beta\,(S_+A_+ - S_-A_-)\,\delta'(t-t'-\frac{\ell}{c})$$

$$+\frac{K}{c}\frac{(z-z')}{\ell\rho^2\rho'^2}\operatorname{csch}\beta\left\{\left[-\operatorname{csch}\beta\coth\beta(2\rho+\rho'+\rho'\cosh\beta)+\rho'+\frac{\rho\rho'(\rho+\rho')}{\ell^2}\right](S_+A_+ - S_-A_-)\right.$$

$$\left.-\frac{\pi}{\alpha}\operatorname{csch}\beta\sinh\frac{\pi\beta}{\alpha}(2\rho+\rho'+\rho'\cosh\beta)(S_+A_+^2 - S_-A_-^2)\right\}\delta(t-t'-\frac{\ell}{c})$$

$$+K\frac{(z-z')}{\rho^3\rho'^3}\operatorname{csch}^2\beta\left\{\left[\rho\operatorname{csch}\beta(2\coth^2\beta+\operatorname{csch}^2\beta)+3\rho'\coth\beta\operatorname{csch}^2\beta\right](S_+A_+ - S_-A_-)\right.$$

$$+\frac{\pi}{\alpha}\left[\rho\operatorname{csch}\beta(3\coth\beta\sinh\frac{\pi\beta}{\alpha}-\frac{\pi}{\alpha}\cosh\frac{\pi\beta}{\alpha})+\rho'(3\coth^2\beta\sinh\frac{\pi\beta}{\alpha}-\frac{\pi}{\alpha}\coth\beta\cosh\frac{\pi\beta}{\alpha}+2\sinh\frac{\pi\beta}{\alpha})\right.$$

$$\left.\left.+2(\frac{\pi}{\alpha})^2\operatorname{csch}\beta\sinh^2\frac{\pi\beta}{\alpha}(\rho+\rho'\cosh\beta)(S_+A_+^3 - S_-A_-^3)\right\}U(t-t'-\frac{\ell}{c}) \tag{48c}$$

$$J_2 = J_1\Big|_{\phi'\to -\phi'} \tag{48d}$$

In (48a), $\delta'(\zeta) = (d/d\zeta)\,\delta(\zeta)$, $r_n \equiv |\underset{\sim}{r}-\underset{\sim}{r}_n|$, $\overline{r}_n \equiv |\underset{\sim}{r}-\overline{\underset{\sim}{r}}_n|$, and it is assumed that $|\phi-\phi_n| \neq \pi$, $|\phi-\overline{\phi}_n| \neq \pi$; (48d) implies that the expression for J_2 is the same as that for J_1 provided that ϕ' is replaced by $-\phi'$. Moreover,

$$S_\pm = \sin\frac{\pi}{\alpha}(\phi-\phi'\mp\pi),\quad A_\pm = \frac{1}{\cosh\frac{\pi\beta}{\alpha}-\cos\frac{\pi}{\alpha}(\phi-\phi'\mp\pi)},\quad K = \frac{c}{8\pi\epsilon\alpha}\ . \tag{48e}$$

These expressions, while derived in a straightforward manner from (47a) and

(47b), are evidently quite involved. For this reason, we shall not write out explicitly the results of the differentiations required for the remaining field components, which are obtained from the following:

$$\hat{E}_{e\phi} = \frac{1}{\rho}\frac{\partial^2}{\partial\phi\partial z}\hat{\Pi}_{ez}, \quad \hat{E}_{ez} = \frac{\partial^2}{\partial z^2}\hat{\Pi}_{ez} - \frac{1}{c^2}\frac{\partial^2}{\partial t^2}\hat{\Pi}_{ez}, \tag{49}$$

$$\hat{H}_{e\rho} = \frac{\epsilon}{\rho}\frac{\partial^2}{\partial\phi\partial t}\hat{\Pi}_{ez}, \quad \hat{H}_{e\phi} = -\epsilon\frac{\partial^2}{\partial\rho\partial t}\hat{\Pi}_{ez}, \quad \hat{H}_{ez} = 0. \tag{50}$$

Longitudinal magnetic dipole

$$\hat{\Pi}_{mz} = \hat{\Pi}^{g}_{mz} + \hat{\Pi}^{d}_{mz} \tag{51}$$

$$\hat{\Pi}^{g}_{mz} = \text{same as (47a), with } \epsilon=1 \text{ and minus sign in front of the second sum changed to plus} \tag{51a}$$

$$\hat{\Pi}^{d}_{mz} = \frac{1}{\epsilon}\hat{G}^{d}_{2} = -\frac{c}{4\pi^2}\frac{\mathrm{Re}\,B(\phi,\phi';-i\beta)+\mathrm{Re}\,B(\phi,-\phi';-i\beta)}{\rho\rho'\sinh\beta}U(t-t'-\frac{\ell}{c}), \tag{51b}$$

where $\hat{G}^{d}_{2}$ is the diffracted part of the scalar Neumann type Green's function [7]. The field components are given in terms of the Hertz potentials by (48a, b), (49) and (50) with the following duality replacements:

$$\hat{\Pi}_e \to \hat{\Pi}_m, \quad \hat{E}_e \to \hat{H}_m, \quad \hat{H}_e \to -\hat{E}_m, \quad \mu \leftrightarrow \epsilon \tag{52}$$

Transverse electric dipole: Special case -- vertical dipole on wedge face $\phi=0$

$$\hat{\underset{\sim}{\Pi}}_e = \hat{\underset{\sim}{\Pi}}^{g}_{e} + \hat{\underset{\sim}{\Pi}}^{d}_{e}, \tag{53}$$

$$\hat{\underset{\sim}{\Pi}}^{g}_{e} = \underset{\sim}{\rho}_o\sum_m \frac{1}{2\pi\epsilon}\frac{\delta(t-t'-r_m/c)}{r_m}\sin(\phi-2m\alpha)\,U(\pi-|\phi-2m\alpha|)$$

$$+\,\underset{\sim}{\phi}_o\sum_m \frac{1}{2\pi\epsilon}\frac{\delta(t-t'-r_m/c)}{r_m}\cos(\phi-2m\alpha)\,U(\pi-|\phi-2m\alpha|) \tag{53a}$$

$$\hat{\Pi}^{d}_{e\rho} = \frac{c}{4\pi\epsilon\alpha\rho\rho'}\sin\frac{\pi\beta}{\alpha}\left[\frac{1}{\cosh\frac{\pi\beta}{\alpha}-\cos\frac{\pi}{\alpha}(\phi-\pi)} - \frac{1}{\cosh\frac{\pi\beta}{\alpha}-\cos\frac{\pi}{\alpha}(\phi+\pi)}\right]U(t-t'-\frac{\ell}{c}) \tag{53b}$$

$$\hat{\Pi}^{d}_{e\phi} = -\frac{c}{4\pi\epsilon\alpha\rho\rho'}\coth\beta\left[\frac{\sin\frac{\pi}{\alpha}(\phi-\pi)}{\cosh\frac{\pi\beta}{\alpha}-\cos\frac{\pi}{\alpha}(\phi-\pi)}-\frac{\sin\frac{\pi}{\alpha}(\phi+\pi)}{\cosh\frac{\pi\beta}{\alpha}-\cos\frac{\pi}{\alpha}(\phi+\pi)}\right]U(t-t'-\frac{\ell}{c}) \tag{53c}$$

Then

$$\hat{H}_{e\rho} = -\epsilon\frac{\partial^2}{\partial t\partial z}\hat{\Pi}_{e\phi}$$

with

$$\hat{H}^{g}_{e\rho} \quad \frac{z-z'}{2\pi}\sum_{m}\left[\frac{1}{cr_m^2}\delta''(t-t'-r_m/c)+\frac{1}{r_m^3}\delta'(t-t'-r_m/c)\right]\cos(\phi-2m\alpha)\,U(\pi-|\phi-2m\alpha|) \tag{54a}$$

$$\hat{H}^{d}_{e\rho}=\frac{\epsilon c^2(t-t')(z-z')}{(\rho\rho')^2}\left[-\operatorname{csch}^2\beta\coth\beta\frac{\partial}{\partial\beta}\hat{\Pi}^{d}_{e\phi}+\operatorname{csch}^2\beta\frac{\partial^2}{\partial\beta^2}\hat{\Pi}^{d}_{e\phi}\right]U(t-t'-\frac{\ell}{c})$$

$$+\frac{\epsilon(z-z')}{\ell\rho\rho'}\left[\ell+c(t-t')\right]\operatorname{csch}\beta\left[\frac{\partial}{\partial\beta}\hat{\Pi}^{d}_{e\phi}\right]\delta(t-t'-\frac{\ell}{c})+\frac{\epsilon}{c}\frac{z-z'}{\ell}\hat{\Pi}^{d}_{e\phi}\,\delta'(t-t'-\frac{\ell}{c}) \tag{54b}$$

The β - derivatives of $\hat{\Pi}^{d}_{e\phi}$ are then calculated from (53c). Similarly,

$$\hat{H}^{g}_{e\phi} = \epsilon\frac{\partial^2}{\partial t\partial z}\hat{\Pi}^{g}_{e\rho} \tag{55a}$$

$\hat{H}^{d}_{e\phi}$ = same as (54b) except that $\hat{\Pi}^{d}_{e\phi}$ is replaced by $\hat{\Pi}^{d}_{e\rho}$ and each term is multiplied by (-1) (55b)

$$\hat{H}_{ez} = \epsilon(\partial/\partial t)[(1/\rho)(\partial/\partial\rho)(\rho\hat{\Pi}_{e\phi})-(1/\rho)(\partial/\partial\phi)\hat{\Pi}_{e\rho}] \tag{56a}$$

$$\hat{H}^{g}_{ez} = \frac{1}{2\pi}\sum_{m}[\rho'-\rho\cos(\phi-2m\alpha)]\left[\frac{1}{cr_m^2}\delta''(t-t'-r_m/c)+\frac{1}{r_m^3}\delta'(t-t'-r_m/c)\right]U(\pi-|\phi-2m\alpha|) \tag{56b}$$

$$\hat{H}^{d}_{ez} = \frac{\epsilon c^2(t-t')}{(\rho\rho')^2}\left\{[\rho\operatorname{csch}^2\beta\coth\beta+\rho'\operatorname{csch}^3\beta]\frac{\partial}{\partial\beta}\hat{\Pi}^{d}_{e\phi}\right.$$

$$\left.-[\rho\operatorname{csch}^2\beta+\rho'\operatorname{csch}\beta\coth\beta]\frac{\partial^2}{\partial\beta^2}\hat{\Pi}^{d}_{e\phi}-\rho'\operatorname{csch}\beta\frac{\partial^2}{\partial\beta\partial\phi}\hat{\Pi}^{d}_{e\rho}\right\}U(t-t'-\frac{\ell}{c})$$

$$-\epsilon\left\{\frac{\operatorname{csch}\beta}{\rho\rho'}[\rho+\rho'\cosh\beta+c(t-t')\frac{\rho+\rho'}{\ell}]\frac{\partial}{\partial\beta}\hat{\Pi}^{d}_{e\phi}+\frac{1}{\rho}\frac{\partial}{\partial\phi}\hat{\Pi}^{d}_{e\rho}\right\}\delta(t-t'-\frac{\ell}{c})$$

$$+\frac{\epsilon(\rho+\rho')}{c\ell}\hat{\Pi}^{d}_{e\phi}\,\delta'(t-t'-\frac{\ell}{c}) \tag{56c}$$

The electric field components are derived in a similar manner. Because the expressions are quite lengthy, we shall not list them in detail:

$$\hat{E}_{e\rho} = \frac{\partial}{\partial\rho}\frac{1}{\rho}\frac{\partial}{\partial\rho}(\rho\,\hat{\Pi}_{e\rho}) + \frac{\partial}{\partial\rho}\frac{1}{\rho}\frac{\partial}{\partial\phi}\hat{\Pi}_{e\phi} - \frac{1}{c^2}\frac{\partial^2}{\partial t^2}\hat{\Pi}_{e\rho} \tag{57}$$

$$\hat{E}_{e\phi} = \frac{1}{\rho^2}\frac{\partial}{\partial\rho}\left(\rho\frac{\partial}{\partial\phi}\hat{\Pi}_{e\rho}\right) + \frac{1}{\rho^2}\frac{\partial^2}{\partial\phi^2}\hat{\Pi}_{e\phi} - \frac{1}{c^2}\frac{\partial^2}{\partial t^2}\hat{\Pi}_{e\phi} \tag{58}$$

$$\hat{E}_{ez} = \frac{1}{\rho}\frac{\partial}{\partial\rho}\left(\rho\frac{\partial}{\partial z}\hat{\Pi}_{e\rho}\right) + \frac{1}{\rho}\frac{\partial^2}{\partial z\partial\phi}\hat{\Pi}_{e\phi} \tag{59}$$

Transverse magnetic dipole: Special case--tangential dipole on wedge face $\phi=0$

The resulting expressions for the potentials and field components are obtained from those for the vertical electric dipole by the following replacements:

$$\epsilon\,\hat{\Pi}_{e\rho} \to \hat{\Pi}_{m\phi}\ , \quad \epsilon\,\hat{\Pi}_{e\phi} \to -\hat{\Pi}_{m\rho} \tag{60}$$

$$\hat{H}_{m\rho} = \text{same as (57) with } \hat{\Pi}_{e\rho,\phi} \to \hat{\Pi}_{m\rho,\phi} \tag{61}$$

$$\hat{H}_{m\phi} = \text{same as (58) with } \hat{\Pi}_{e\rho,\phi} \to \hat{\Pi}_{m\rho,\phi} \tag{62}$$

$$\hat{H}_{mz} = \text{same as (59) with } \hat{\Pi}_{e\rho,\phi} \to \hat{\Pi}_{m\rho,\phi} \tag{63}$$

$$\hat{E}_{m\rho} = \mu\frac{\partial^2}{\partial t\partial z}\hat{\Pi}_{m\phi}\ , \quad \hat{E}_{m\phi} = -\mu\frac{\partial^2}{\partial t\partial z}\hat{\Pi}_{m\rho} \tag{64}$$

$$\hat{E}_{mz} = -\mu\frac{\partial}{\partial t}\left[\frac{1}{\rho}\frac{\partial}{\partial\rho}(\rho\,\hat{\Pi}_{m\phi}) - \frac{1}{\rho}\frac{\partial}{\partial\phi}\hat{\Pi}_{m\rho}\right] \tag{65}$$

V. Simplifications for Special Cases

To check the validity of the results derived in Section IV, we have considered two special cases, which have been treated previously by other methods. In the first case, the incident pulse is planar instead of spherical while in the second case, the spherical pulse strikes a half plane ($\alpha = 2\pi$).

1. Incident plane pulse

When the location of an impulsive point source is moved to infinity, the incident spherical wavefront appears planar in any finite observation region. To assure that the incident field is non-vanishing, the source strength must be increased appropriately; moreover, the time reference must be shifted from the turn-on time of the dipole in order to eliminate parameters descriptive of the infinite travel time from the source to the observation point.

These considerations are evident from an examination of the functions that characterize spherical and plane pulses. For a scalar spherical pulse originating at $\underset{\sim}{r}' = (\rho', \phi', z')$,

$$\hat{G}(\underset{\sim}{r}, \underset{\sim}{r}'; t, t') = \frac{\delta[t-t'-|\underset{\sim}{r}-\underset{\sim}{r}'|/c]}{4\pi|\underset{\sim}{r}-\underset{\sim}{r}'|} , \tag{66}$$

where in the plane $z=z'$,

$$|\underset{\sim}{r}-\underset{\sim}{r}'| = [\rho^2 + \rho'^2 - 2\rho\rho' \cos(\phi-\phi')]^{\frac{1}{2}} , \quad z=z' . \tag{67}$$

As the source point is moved to infinity in the ϕ'- direction in the plane $z=z'$, one has

$$|\underset{\sim}{r}-\underset{\sim}{r}'| \sim \rho' - \rho \cos(\phi-\phi') + 0(\frac{1}{\rho'}) , \quad \rho' \to \infty , \tag{68}$$

so that

$$\hat{G}_{inc} \sim \frac{\delta[t+ (\rho/c) \cos(\phi-\phi') - t' - \rho'/c]}{4\pi\rho'} , \quad \rho' \to \infty . \tag{69}$$

A plane pulse incident along the direction $\phi=\phi'$ is usually described by

$$\hat{u}_{inc} \sim \delta[t+(\rho/c) \cos(\phi-\phi')] , \tag{70}$$

implying that time $t=0$ corresponds to the instant when the wavefront passes

through the origin $\rho=0$. Comparing (69) and (70), one obtains the following prescription for converting a spherical pulse solution $\hat{G}(\underset{\sim}{r}, \underset{\sim}{r}'; t, t')$ into a plane pulse solution $\hat{u}(\underset{\sim}{r}, \phi', t)$:

$$\hat{u}(\underset{\sim}{r}, \phi', t) = \lim_{\rho' \to \infty} [4\pi\rho' \hat{G}(\underset{\sim}{r}, \underset{\sim}{r}'; t, -\frac{\rho'}{c})] . \tag{71}$$

The limiting operation is now performed on the solution for a pulsed vertical electrical dipole on the $\phi'=0$ wedge face. We identify $\hat{G}$ in (71) with the magnetic field component $\hat{H}_{ez}(\underset{\sim}{r}, \underset{\sim}{r}'; t, t')$, and calculate first the incident field. As the dipole is moved to infinity and the limit is calculated according to (71), one obtains from (56a) on omitting the image contributions:

$$\hat{u}_{inc} = \frac{1}{c} \frac{\partial^2}{\partial t^2} \delta(t + \frac{\rho \cos \phi}{c}) \quad . \tag{72}$$

Since the incident field is the conventional scalar plane pulse operated on by $(\partial^2/c\partial t^2)$, the limiting form of the spherical pulse solution should be the known plane pulse solution subjected to the same operator. Indeed, we find from (56a) that the limiting geometric-optical field is:

$$\hat{u}^g = \frac{1}{c} \frac{\partial^2}{\partial t^2} \left\{ 2 \sum_n \delta(t + \frac{\rho \cos(\phi - 2m\alpha)}{c}) \, U(\pi - |\phi - 2m\alpha|) \right\} \quad . \tag{73}$$

Concerning the diffraction field in (56b), we note first that the operation $\rho' \to \infty$, with $ct' = -\rho'$, yields

$$\beta = \cosh^{-1} \left[\frac{c^2(t-t')^2 - \rho^2 - \rho'^2 - (z-z')^2}{2\rho\rho'} \right] \to \cosh^{-1} (\frac{ct}{\rho}). \tag{74}$$

Then one may show that :

$$\hat{u}^d = \frac{1}{c} \frac{\partial^2}{\partial t^2} \left\{ -2 \frac{2}{\pi} \frac{\mathrm{Re}\, B(\phi, 0; -i\beta)}{\sqrt{(t-t')^2 - (\rho/c)^2}} \, U(t-t' - \rho/c) \right\} \quad . \tag{75}$$

The expressions inside the braces in (73) and (75) are the correct plane pulse solutions as given in [7].

2. Half Plane

When the wedge degenerates into a half plane ($\alpha=2\pi$), the general solutions in Sec. IV. 2 simplify substantially. An interesting form of the

vector Hertz potential due to an arbitrarily oriented pulsed dipole in the presence of a perfectly conducting half plane has been presented recently [4]. It was shown that the Hertz vectors $\hat{\underset{\sim}{\Pi}}_e$ or $\hat{\underset{\sim}{\Pi}}_m$ can be obtained as a superposition of three contributions. The first two involve respectively the Dirichlet and Neumann scalar Green's functions while the third resembles the form ot a line source field originating at the edge. The third contribution is required to satisfy the edge condition on the vector field when the dipole sourcc has transverse components; this cannot be accomplished by use of only thc two scalar Green's functions. We shall first show how certain terms in our general solution for a transverse electric dipole reduce when $\alpha=2\pi$, and we shall then cast the reduced solution into the form described above.

Setting $\alpha=2\pi$, one has from (46a) that

$$Q_1(\varphi, w) = - \cos(\varphi-w) \cot\frac{\varphi-w-\pi}{4} + \cos(\varphi+w) \cot\frac{\varphi+w+\pi}{4}. \tag{76}$$

Then setting $w=-i\beta$, using the identity

$$\cot(x+iy) = \frac{\sin 2x - i \sinh 2y}{\cosh 2y - \cos 2x} , \tag{77}$$

and simplifying, one finds that

$$\text{Re } Q_1(\varphi, -i\beta) = 4 \cos\frac{\varphi}{2} \cosh\frac{\beta}{2} - 4 \text{ Re } B(\varphi, -i\beta) , \tag{78}$$

where

$$\text{Re } B(\varphi, -i\beta) = \frac{\cosh\frac{\beta}{2} \cos\frac{\varphi}{2}}{2(\cosh^2\frac{\beta}{2} - \sin^2\frac{\varphi}{2})} . \tag{78a}$$

Also, from (46b), with $\alpha=2\pi$,

$$\text{Re } Q_2(\varphi, -i\beta) = 4 \sin\frac{\varphi}{2} \cosh\frac{\beta}{2} . \tag{79}$$

When these expressions are substituted into (44), one may derive the following form for the diffracted components of the Hertz vector:

$$\hat{\Pi}^d_{ex} = \frac{1}{\epsilon} \cos\nu_e \, \hat{G}^d_1(\underset{\sim}{r}, \underset{\sim}{r}'; t, t')$$

$$+ \frac{1}{4\pi\epsilon} \frac{2c}{\pi} \frac{\cosh\frac{\beta}{2}}{\rho\rho' \sinh\beta} \left[\sin\frac{\phi}{2} \sin\frac{\phi'}{2} \cos\nu_e - \sin\frac{\phi}{2} \cos\frac{\phi'}{2} \sin\nu_e \right] U(t-t'-\frac{\ell}{c}) \tag{80}$$

$$\hat{\Pi}^d_{ey} = \frac{1}{\epsilon} \sin \nu_e \, \hat{G}^d_2(\underset{\sim}{r}, \underset{\sim}{r}'; t, t')$$

$$+ \frac{1}{4\pi\epsilon} \frac{2c}{\pi} \frac{\cosh \frac{\beta}{2}}{\rho\rho' \sinh \beta} \left[- \cos\frac{\phi}{2} \sin\frac{\phi'}{2} \cos \nu_e + \cos\frac{\phi}{2} \cos\frac{\phi'}{2} \sin \nu_e \right] U(t-t'-\frac{\ell}{c}), \tag{81}$$

where $\hat{G}^d_1$ and $\hat{G}^d_2$ are the diffracted parts of the scalar Dirichlet and Neumann Green's functions given in (47b) and (51b), respectively, with Re $B(\phi, \pm\phi'; -i\beta)$ in (47c) replaced by Re $B(\phi \mp \phi', -i\beta)$ in (78a). Moreover, since

$$\sinh\frac{\beta}{2} = \left(\frac{\cosh\beta - 1}{2}\right)^{\frac{1}{2}} = \left[\frac{c(t-t')^2 - (\rho+\rho')^2 - (z-z')^2}{4\rho\rho'}\right]^{\frac{1}{2}}$$

$$= \frac{c}{2\sqrt{\rho\rho'}} \sqrt{(t-t')^2 - (\ell/c)^2} \tag{82}$$

one may eliminate $\cosh(\beta/2)\,(\sinh\beta)^{-1} = [2\sinh(\beta/2)]^{-1}$ via (82). Recalling that the scalar line source Green's function is [7]

$$\hat{G}_\ell(\underset{\sim}{\rho}, \underset{\sim}{\rho}', t, t') = \frac{1}{2\pi\left[(t-t')^2 - |\underset{\sim}{\rho} - \underset{\sim}{\rho}'|^2/c^2\right]^{\frac{1}{2}}} U\left[(t-t') - \frac{|\underset{\sim}{\rho} - \underset{\sim}{\rho}'|}{c}\right] \tag{83}$$

one identifies the second terms in (80) and (81) as the previously mentioned contributions due to a virtual line source at the edge. When the geometric-optical contributions are added, one finds that $\hat{\Pi}_{ex}$ and $\hat{\Pi}_{ey}$ are given by (80) and (81), respectively, provided that $\hat{G}^d_1$ and $\hat{G}^d_2$ are replaced by the complete scalar Green's functions $\hat{G}_1$ and $\hat{G}_2$. The resulting expressions then agree with those in [4], except for a factor accounting for a different normalization employed here.

VI. Simulation of an Incident Plane Pulse

In order to examine the effect of an electromagnetic pulse on various structures and equipment, it is necessary to produce a suitable pulse form. Ideally, we would like to be able to produce a step function electromagnetic wave, i.e. an electric field that, at every point in space, is zero until time t(x, y, z) and then instantaneously changes to a fixed vector value $\underset{\sim}{E}_o$; the corresponding magnetic field should change similarly at time t from 0 to $\underset{\sim}{H}_o$, the directions of $\underset{\sim}{E}_o$, $\underset{\sim}{H}_o$ and ∇t being mutually perpendicular, with the magnitudes of $\underset{\sim}{E}_o$, $\underset{\sim}{H}_o$ related by the intrinsic impedance of free space. In principle, such a field distribution can be produced by crossed electric and magnetic dipoles whose source strength varies quadratically with time, provided that the test region is very far from the dipole location. In practice, that distance is not very large, with the unfortunate consequence that the field amplitude cannot then be independent of position. Nevertheless, we shall show that it is possible to simulate plane wave behavior at a point. With a suitably designed, physically realizable, electric dipole alone it is possible to produce a step-function electric field while with crossed electric and magnetic dipoles, it is possible to synthesize step function electric and magnetic fields, at right angles to each other and related by the free space impedance [9]. A brief discussion of a possible method of realization of such an excitation will be given. Finally, the inhomogeneity of the field distribution will be examined, so that the size of a usable test region can be estimated.

1. Electric dipole excitation

Let us consider the electromagnetic field in vacuum* due to a z-directed electric dipole whose moment is p(t). We obtain at (r, θ, ϕ) in a spherical coordinate system [10]

$$\hat{E}_\theta(t+r/c) = \frac{\zeta \sin\theta}{4\pi r}\left(\frac{p''}{c} + \frac{p'}{r} + \frac{cp}{r^2}\right) \tag{84a}$$

$$\hat{H}_\phi(t+r/c) = \frac{\sin\theta}{4\pi r}\left(\frac{p''}{c} + \frac{p'}{r}\right) \tag{84b}$$

$$\hat{E}_r(t+r/c) = \frac{2\cos\theta}{4\pi r^2 \epsilon_o}\left(\frac{p'}{c} + \frac{p}{r}\right) \tag{84c}$$

where p' and p'' denote the first and second time derivatives of the dipole moment p(t), $c=(\epsilon_o\mu_o)^{-\frac{1}{2}}$ is the velocity of light, $\zeta=(\mu_o/\epsilon_o)^{\frac{1}{2}}$ is the free space impedance. The dipole is switched on at t=0. Alternatively, the same fields can be

*Note that the coordinate system employed in this section is not related to the wedge-centered coordinate system employed in Secs. II-V.

generated by a current element i(t) (i denotes the product of current and length of a short dipole, or in a volume current density distribution $j_z = \delta(\underset{\sim}{r})\, i(t)$):

$$i(t) = p'(t). \tag{85}$$

We can now ask what function p(t) will yield an electric field at $(a, \pi/2, 0)$, which has a step function behavior. Since $\hat{E}_r = 0$ for $\theta = \pi/2$, we set

$$\hat{E}_\theta(a, \pi/2, 0) = E_o\, U(t) \tag{86}$$

where U(t) is the unit step function with t measured from the time of arrival of the wave at the observation point. Thus we seek the solution of the differential equation

$$(\zeta/4\pi ac)\left[p'' + (c/a)p' + (c/a)^2 p\right] = E_o\, U(t), \tag{87}$$

subject to the initial condition $p' = p = 0$ at $t=0$. Solving this equations, we obtain

$$p(t) = 4\pi \varepsilon_o a^3 E_o U(\tau)\left[1 - e^{-\tau/2}\left(\cos\frac{\sqrt{3}\,\tau}{2} + \frac{1}{\sqrt{3}}\sin\frac{\sqrt{3}\,\tau}{2}\right)\right]$$

$$= 4\pi \varepsilon_o a^3 E_o U(\tau)\left[1 - \frac{2}{\sqrt{3}} e^{-\tau/2}\sin\left(\frac{\pi}{3} + \frac{\sqrt{3}\,\tau}{2}\right)\right] \tag{88}$$

where $\tau = ct/a$.

The corresponding variation of i(t) and $\hat{H}_\phi$ is

$$i(t) = (8\pi a^2/\zeta\sqrt{3})\, E_o U(\tau)\, e^{-\tau/2} \sin(\sqrt{3}\,\tau/2) \tag{89}$$

$$\hat{H}_\phi = (E_o/\zeta)\, e^{-\tau/2}\left(\cos\frac{\sqrt{3}\,\tau}{2} + \frac{1}{\sqrt{3}}\sin\frac{\sqrt{3}\,\tau}{2}\right) \tag{90}$$

The seemingly arbitrary choice of $\theta = \pi/2$ at the field point is due to the fact that the radial component of the electric field vanishes there and, in addition, the θ - derivative of $\hat{E}_\theta$ vanishes, thus assuring maximum homogeneity of the electric field distribution.

The temporal variation of $\hat{E}_\theta$, $\hat{H}_\phi$, p and i is shown in Fig. 4. We see that the magnetic field begins to deviate significantly from (E_o/ζ) at times less than (a/c) after wavefront arrival and, for all practical purposes, vanishes for $t > 6a/c$. In order to overcome this difficulty, an additional magnetic dipole is necessary. We may note that as "a" increased, the time axis is stretched out and, for a long time, the desired p(t) behavior is parabolic.

2. Electric and magnetic dipole excitation

In order to achieve step function behavior for both electric and magnetic fields, we must introduce another degree of freedom in the source function - -a magnetic dipole whose time dependence is to be determined. This dipole must be oriented at right angles to the electric dipole and to the radius vector from the source to the field point in order that it contribute to the same field components as the electric dipole. The source is then described by the electric dipole $\underset{\sim}{P}$ and magnetic dipole $\underset{\sim}{M}$ given by

$$\underset{\sim}{P} = p(t)\, \delta(\underline{r})\, \underset{\sim}{z}_o \tag{91a}$$

and

$$\underset{\sim}{M} = m(t)\, \delta(\underline{r})\, \underset{\sim}{y}_o \quad . \tag{91b}$$

In this case we obtain a pair of coupled differential equations for p(t) and m(t) by equating (in Cartesian coordinates)

$$\hat{E}_z(a,0,0) = - E_o\, U(t) \tag{92a}$$

$$\hat{H}_y = (E_o/\zeta)\, U(t) \tag{92b}$$

where t is again measured from the time of arrival of the wavefront. These differential equations are

$$[p + (a/c)\, p' + (a/c)^2 p''] - (1/c)\, [(a/c)m' + (a/c)^2 m''] = 4\pi \epsilon_o a^3 E_o U(t) \tag{93a}$$

$$[(a/c)p' + (a/c)^2 p''] - 1/c[m + (a/c)m' + (a/c)^2 m''] = 4\pi \epsilon_o a^3 E_o U(t). \tag{93b}$$

From these equations, as well as directly from the symmetry of the problem, it follows that

$$p(t) = - m(t)/c \tag{94}$$

and the system (93) reduces to the second order equation

$$p + 2(a/c)p' + 2(a/c)^2 p'' = 4\pi \epsilon_o a^3 E_o\, U(t) \quad . \tag{95}$$

The solution of this equation is

$$p(t) = 4\pi \epsilon_o a^3 E_o \left\{1 - \exp(-\tau/2)[\sin(\tau/2) + \cos(\tau/2)]\right\}$$

$$= 4\pi \epsilon_o a^3 E_o \left\{1 - \sqrt{2} \exp(-\tau/2) \sin(\tau/2 + \pi/4)\right\} \tag{96a}$$

$$m(t) = - c\, p(t) \quad . \tag{96b}$$

This combination of electric and magnetic crossed dipoles will produce at the point (a,0 , 0) an electromagnetic field perfectly simulating that of plane wave.

3. Waveform realization

In attempting to synthesize the required p(t) variation, we can proceed on the assumption that, from a circuit point of view, the dipole is a capacitive structure, with the dipole moment proportional to the capacitor voltage. Consider then the network shown in Fig. 5, consisting of the dipole structure with capacitance C_d, a charged condenser C_s, which is connected to the dipole by a series switch, an inductance L, and a resistance R. The initial values of the voltage across C_d, and its first derivative, are zero, as is required for p(t). Hence if the inductance and resistance are adjusted to make the complex resonance frequency $\omega = \frac{c}{2a}(1-i)$ for the transient given by (96)and $\omega = \frac{c}{2a}(\sqrt{3} - i)$ for that given by (88), then a step function field is obtained. The resonant period of the circuit must be of the order of magnitude of the time of travel of the wave from the source to the observation point. This circuit is a modification of one given by Baum [9]. Using the resonant frequencies above in the circuit of Fig. 5 and assuming C_s and C_d to be given, one finds from the resonance condition

$$\frac{1}{-i\omega C} + R - i\omega L = 0 , \qquad C = \frac{1}{C_s} + \frac{1}{C_d} , \tag{97}$$

that for the transient in (96),

$$R = \frac{2}{C}\,\frac{a}{c} , \qquad L = \frac{2}{C}\left(\frac{a}{c}\right)^2 , \tag{98a}$$

while for the transient in (88),

$$R = \frac{1}{C}\,\frac{a}{c} , \qquad L = \frac{1}{C}\left(\frac{a}{c}\right)^2 . \tag{98b}$$

The design of a suitable generator circuit for a magnetic dipole is more difficult but again, circuits discussed in [10] can be used, with the proviso that resonant frequencies and damping rates be suitably adjusted for source proximity.

4. Field amplitude homogeneity

Although no exhaustive study of field variation was performed, there are reasons to believe that the primary limitation is the $1/R^3$ field dependence of a static dipole. The electric field on the x axis was calculated and found to be

$$\hat{E}_z = - E_o \left(\frac{a}{x}\right)^3 \left\{ 1 - e^{-\tau/2} \left[\left(1 - \frac{x}{a}\right)^2 \sin \frac{\tau}{2} + \left(1 - \frac{x^2}{a^2}\right) \cos \frac{\tau}{2} \right] \right\} \qquad (99)$$

We see that, for large τ, the static dipole result mentioned above is evident. For $|x-a| \ll a$ the fractional change in field amplitude is $3|x-a|/a$. The initial response, for $\tau \to 0$, is proportional to (a/x), so that the fractional change is only $|x-a|/a$. Numerical examination of (99) for (x/a) close to unity shows that, as a function of τ, there is a gradual transition from the relatively weak initial inhomogeneity to the static field inhomogeneity. Since there are no first order inhomogeneity effects in the transverse directions, it is expected that the limitation due to x-dependence will be the limiting factor.

VII. Numerical Results

Carefully tested numerical results for three selected special cases of wedge angle and observation angle are plotted in Figs. 6(a) - (c), for excitation by a vertical electric dipole. The dipole moment is the function given in (88), with $a = \rho'$, i.e., the incident electric field at the edge behaves like a unit step function. In each figure, the temporal field variation in the plane $z = z'$ is shown for $\rho = 0.01$ and $\rho = 0.2$, with $\rho' = 1$ (see also Appendix C, Sec. 6). Here, ρ and ρ' denote normalized distances; unnormalized results are obtained by interpreting ρ as the ratio of edge-to-observation-point to edge-to-source-point distance. The case $\rho = 0.01$ represents a very distant source, and the fields should thus be nearly identical with those for an incident plane pulse. The curves obtained for $\rho = 0.01$ do, in fact, show agreement with previously obtained results for the plane wave case [2] and this check confirms the correctness of the computer program.

We can now assess the effect of dipole proximity near the edge by comparing the $\rho = 0.2$ curve with the quasi-plane-wave case, $\rho = 0.01$, in each plot. The electric and magnetic fields are normalized to the (unit amplitude) field discontinuity across the wavefront at the edge, and time $t = 0$ corresponds to the time of arrival of the incident field at the observation point. For $\rho = 0.01$, the observation point is near the edge and near the wedge face whereon the dipole is situated; therefore, the incident $\hat{E}_y$ and $\hat{H}_z$ fields behave almost as those in a plane pulse (see Fig. 6(b)). For $\rho = 0.2$ in Fig. 6(b), the observation point is sufficiently far removed from the edge and the dipole plane to exhibit noticeable deviations of the incident fields from those of a plane pulse. These deviations of the incident and also reflected fields (initial portions of the curves in Figs. 6(b) and 6(c)) are $O(\rho/\rho')$, as is to be expected from the discussion in Sec. VI.4. The diffracted fields (curved portions of the graphs) differ by a similar amount over the initial period following the arrival of the diffracted wavefront. However, the long-time behavior for $\rho = 0.2$ can deviate more significantly from that for $\rho = 0.01$.

The three configurations in Figs. 6 differ as follows: in Fig. 6(a) only the diffracted field reaches the observation point; in Fig. 6(b), the incident and diffracted fields are present; and in Fig. 6(c), the observation point is reached by incident, reflected and diffracted waves. The order of magnitude of the proximity effect within the time interval under consideration is substantially the same in all three cases. Further examples of transient field behavior are shown on Figs. 7-26, for wedge angles ranging from 135° to 270°. For small values of ρ/ρ' the proximity effect, i.e. the change in the diffracted field, is of the order of (ρ/ρ'). We see that there are locations in which the field appears to vary much less than in the plane wave incidence case. For example, the 270° wedge region (Fig. 10) seems to provide a region in which the field remains relatively constant over a time range.

Appendix A.

Summing the image series

When the image solutions in (39) and (40) are superimposed to satisfy the boundary conditions for a perfectly conducting wedge, one encounters infinite series which are typefied by the one for $A_x^{(1)}(\phi, \phi', w)$ derived from (39a):

$$A_x^{(1)}(\phi, \phi', w) = \sum_{n=-\infty}^{\infty} \left[\frac{1}{\pi - |\phi - (2n\alpha + \phi')| - w} + \frac{1}{\pi + |\phi - (2n\alpha + \phi')| + w} \right] \cos(2n\alpha + \nu_e). \tag{A1}$$

Important in subsequent manipulations is the recognition that only the even part in w of the function $A_x^{(1)}$ contributes to the integral in (36). Therefore, we may change w into -w, or omit odd functions in w, without affecting the value of the resulting integral.

For $n > 0$ and $\phi > \phi'$, we have

$$\pi - |\phi - (2n\alpha + \phi')| - w = \pi - 2n\alpha + (\phi - \phi') - w \tag{A2a}$$

$$\pi + |\phi - (2n\alpha + \phi')| + w = \pi + 2n\alpha - (\phi - \phi') + w \tag{A2b}$$

while for $n < 0$ and $\phi > \phi'$,

$$\pi - |\phi - (2n\alpha + \phi')| - w = \pi + 2n\alpha - (\phi - \phi') - w \tag{A3a}$$

$$\pi + |\phi - (2n\alpha + \phi')| + w = \pi - 2n\alpha + (\phi - \phi') + w \tag{A3b}$$

Changing w into -w in (A2a) and (A3a), we may regroup the images and obtain the following expression for the series in (A1):

$$A_x^{(1)}(\phi, \phi', w) = \frac{1}{2\alpha} \sum_{n=-\infty}^{\infty} \frac{\cos(2n\alpha + \nu_e)}{n - \frac{(\phi - \phi') - w - \pi}{2\alpha}} - \frac{1}{2\alpha} \sum_{n=-\infty}^{\infty} \frac{\cos(2n\alpha + \nu_e)}{n - \frac{(\phi - \phi') + w + \pi}{2\alpha}} . \tag{A4}$$

Writing

$$\cos(2n\alpha + \nu_e) = \cos(2n\alpha) \cos \nu_e - \sin(2n\alpha) \sin \nu_e, \tag{A5}$$

one observes that the series in (A4) are of the kind shown on the left-hand sides of (41a, b), and are therefore given by the closed forms on the right-hand sides. Thus,

$$A_x^{(1)} = -\frac{\pi}{2\alpha}\cos\nu_e\left\{\frac{\cos[(2\alpha-\pi)\varphi_-]}{\sin[\pi\varphi_-]} - \frac{\cos[(2\alpha-\pi)\varphi_+]}{\sin[\pi\varphi_+]}\right\}$$

$$+\frac{\pi}{2\alpha}\sin\nu_e\left\{\frac{\sin[(2\alpha-\pi)\varphi_-]}{\sin[\pi\varphi_-]} - \frac{\sin[(2\alpha-\pi)\varphi_+]}{\sin[\pi\varphi_+]}\right\} \qquad \text{(A6)}$$

where

$$\varphi_- = \frac{\phi - \phi' - w - \pi}{2\alpha}, \quad \varphi_+ = \frac{\phi - \phi' + w + \pi}{2\alpha} \qquad \text{(A6a)}$$

Consider now the expression inside the first braces in (A6):

$$\{\ \} = \cos(\phi-\phi'-w-\pi)\cot[\pi\varphi_-] + \sin(\phi-\phi'-w-\pi)$$

$$-\cos(\phi-\phi'+w+\pi)\cot[\pi\varphi_+] - \sin(\phi-\phi'+w+\pi) \qquad \text{(A7)}$$

Combining the two sine functions, one obtains $\cos(\phi-\phi')\sin w$, i.e., an odd function in w, which does not contribute to the integral in (36). Therefore, only the first and third terms in (A7) are significant. An analogous simplification is obtained for the expression inside the second braces in (A6).

The image sums derived from (39b), (40a) and (40b) are treated in a similar manner.

Appendix B

Expressions for the Fields near the Plane $z=z'$

The exact expressions for the field components in Sec. IV.2 simplify when the fields are evaluated in the source plane $z=z'$. To explore the field behavior near the plane $z=z'$, we have examined the power series expansion

$$B(\underset{\sim}{\rho}, z, \underset{\sim}{\rho}', z'; t, t') = B\Big|_{z=z'} + \frac{\partial B}{\partial z}\Big|_{z=z'} (z-z') + \frac{1}{2}\frac{\partial^2 B}{\partial z^2}\Big|_{z=z'} (z-z')^2 + \ldots . \tag{B1}$$

where B stands for any of the field components. For the vertical electric dipole located on the wedge face $\phi=0$, one has

$$H_\rho = H_\phi = E_z = 0 \qquad \text{when} \quad z=z', \tag{B2}$$

whence these field components behave like $(\partial B/\partial z)_{z=z'}(z-z')$ near $z=z'$. The remaining field components H_z, E_ρ, E_ϕ are finite when $z=z'$ and have vanishing first derivatives at $z=z'$, whence the corrections for $z \approx z'$ to their values at $z=z'$ are $0[(z-z')^2]$; this requires evaluation of the second derivatives of the field components and leads to expressions that are no simpler than the exact ones. Therefore, nothing is gained by explicit analytical calculation of the approximate forms for H_z, E_ρ and E_ϕ.

Even the expressions for H_ρ, H_ϕ and E_z turn out to be fairly complicated. One obtains for observation points off the wavefront:

$$\frac{\partial H_\rho}{\partial z}\Big|_{z=z'} = \frac{\epsilon c^2 (t-t')}{(\rho\rho')^2}\left[-\operatorname{csch}^2\beta \coth\beta \frac{\partial \hat{\Pi}_{e\phi}}{\partial\beta} + \operatorname{csch}\beta \frac{\partial^2 \hat{\Pi}_{e\phi}}{\partial\beta^2}\right]_{z=z'} \tag{B3}$$

$$\frac{\partial H_\phi}{\partial z}\Big|_{z=z'} = \frac{\epsilon c^2 (t-t')}{(\rho\rho')^2}\left[-\operatorname{csch}^2\beta \coth\beta \frac{\partial \hat{\Pi}_{e\rho}}{\partial\beta} + \operatorname{csch}^2\beta \frac{\partial^2 \hat{\Pi}_{e\rho}}{\partial\beta}\right]_{z=z'} \tag{B4}$$

$$\frac{\partial E_z}{\partial z}\Big|_{z=z'} = -\frac{1}{(\rho\rho')^2}\left\{\left[\rho \operatorname{csch}^2\beta\coth\beta + \rho' \operatorname{csch}^3\beta\right]\frac{\partial \hat{\Pi}_{e\rho}}{\partial\beta} - \left[\rho\operatorname{csch}^2\beta + \rho'\operatorname{csch}\beta\coth\beta\right]\frac{\partial^2 \hat{\Pi}_{e\rho}}{\partial\beta^2} + \rho'\operatorname{csch}\beta \frac{\partial^2 \hat{\Pi}_{e\phi}}{\partial\phi\,\partial\beta}\right\}_{z=z'} \tag{B5}$$

where

$$\left.\frac{\partial \hat{\Pi}_{e\phi}}{\partial \beta}\right|_{z=z'} = \left[\operatorname{csch}^2\beta \sin\frac{\pi}{\alpha}(\phi-\pi)A(\phi)+\frac{\pi}{\alpha}\coth\beta \sinh\frac{\pi\beta}{\alpha}\sin\frac{\pi}{\alpha}(\phi-\pi)\,A^2(\phi)\right]_{z=z'}+(\phi\rightarrow-\phi) \tag{B6}$$

$$\left.\frac{\partial^2 \hat{\Pi}_{e\phi}}{\partial \beta^2}\right|_{z=z'} = \left[-2\operatorname{csch}^2\beta\coth\beta\,A(\phi) - \frac{2\pi}{\alpha}\operatorname{csch}^2\beta\sinh\frac{\pi\beta}{\alpha}A^2(\phi)\right.$$

$$\left. + \left(\frac{\pi}{\alpha}\right)^2\coth\beta\cosh\frac{\pi\beta}{\alpha}A^2(\phi) - 2\left(\frac{\pi}{\alpha}\right)^2\coth\beta\sinh^2\frac{\pi\beta}{\alpha}A^3(\phi)\right]_{z=z'}\sin\frac{\pi}{\alpha}(\phi-\pi)+(\phi\rightarrow-\phi) \tag{B7}$$

$$\left.\frac{\partial \hat{\Pi}_{e\rho}}{\partial \beta}\right|_{z=z'} = \left[\frac{\pi}{\alpha}\cosh\frac{\pi\beta}{\alpha}A(\phi) - \frac{\pi}{\alpha}\sinh^2\frac{\pi\beta}{\alpha}A^2(\phi)\right]_{z=z'} - (\phi\rightarrow-\phi) \tag{B8}$$

$$\left.\frac{\partial^2 \hat{\Pi}_{e\rho}}{\partial \beta^2}\right|_{z=z'} = \left(\frac{\pi}{\alpha}\right)^2\left[\sinh\frac{\pi\beta}{\alpha}A(\phi) - 3\sinh\frac{\pi\beta}{\alpha}\cosh\frac{\pi\beta}{\alpha}A^2(\phi)+2\sinh^3\frac{\pi\beta}{\alpha}A^3(\phi)\right]_{z=z'}-(\phi\rightarrow-\phi) \tag{B9}$$

$$\left.\frac{\partial^2 \hat{\Pi}_{e\rho}}{\partial \phi\,\partial \beta}\right|_{z=z'} = -\left(\frac{\pi}{\alpha}\right)^2\left[\cosh\frac{\pi\beta}{\alpha}\sin\frac{\pi}{\alpha}(\phi-\pi)A^2(\phi)-2\sinh^2\frac{\pi\beta}{\alpha}\sin\frac{\pi}{\alpha}(\phi-\pi)A^3(\phi)\right]_{z=z'}+(\phi\rightarrow-\phi) \tag{B10}$$

In these equations, $(\phi\rightarrow-\phi)$ denotes the preceding terms with ϕ replaced by $-\phi$.

Appendix C

1. The Computer Program

The analytical results obtained in the preceding sections hold for the most general situation, e.g., regardless of the wedge angle or the source location and orientation. The present computer program is, however, developed only for the special case where an electric dipole is situated on and perpendicular to the surface of the wedge at $\varphi = 0$. The reason for doing this will be explained subsequently.

As shown in Section IV, the electromagnetic field can be subdivided into geometric optical and diffracted fields. The geometric optical field can be simply and directly accounted for, even in the case of a dipole with arbitrary time variation. On the other hand, the diffracted field is analyzed through the vector Hertz potential. Furthermore, for a source of arbitrary time variation, the field is determined by the convolution of the source function with the time-dependent Green's functions obtained in Section IV. Since no analytic result is expected for the convolution integrals encountered here, they are evaluated numerically. It is this numerical evaluation of convolution integrals that consumes substantial computer time and space, especially for long observation times. For this reason, the scope of the computer program has to be restricted. It should be pointed out, however, that if the computer time and space are not of primary concern, the present program can be modified for the general case without major effort.

A number of "comment" statements are provided in the program and the output data are all under appropriate labellings. Therefore, the program should be easy to read and interpret.

2. The Computational Scheme

The numerical computation of the electromagnetic field due to a time varying dipole in the presence of a perfectly conducting wedge can be subdivided into the relatively simple computation of the incident and geometrically reflected fields and the more complicated evaluation of the diffracted field. The diffracted field is obtained by making use of the expressions for the vector Hertz potentials obtained in Section IV. 2. We could proceed by calculating first the electromagnetic field of an impulsive (delta function) dipole and then convolve

this response with the time variation of the actual dipole or, alternatively, we could first convolve the Hertz potentials with the dipole time variation and then differentiate these to obtain the electromagnetic field. The latter approach was taken in order to reduce the singularity of the functions to be differentiated. Proceeding the other way necessitates the analytic separation of singular terms from the solution, the differentiation and integration of these terms, and subsequent combination of these analytic results with the corresponding results obtained by numerical integration and differentiation of the well-behaved part of the solutions.

The choice of the "convolution first - differentiation second" approach necessitated an immediate decision concerning the dipole time dependence. For this reason, the electric dipole producing a step-function electric field at the edge of the wedge (cf. Section VI) was selected. This dipole moment time variation appears in the computer program as function PN(TA); it also appears indirectly in the expressions for the incident and reflected fields. These expressions would have to be modified if a different dipole moment time dependence were to be used. For a vertical electric dipole on the wedge face $\phi = 0$, the dipole orientation is along ϕ and the location was chosen at $(\rho, \phi, z) = (1, 0, 0)$.

The numerical computation proceeds by calculation of the radial and angular components of the Hertz potentials at the observation point $(\rho, \phi_c, 0)$, and at a number of neighboring points in order to provide for numerical differentiation. These differentiations are then carried out, and the diffracted electromagnetic field is calculated. The diffracted field is then added to the corresponding field of the dipole and its image. It is assumed that no more than a single image dipole contributes; this restricts the exterior wedge angle α to the range $\alpha > \pi/2$; should the need arise, a modification for smaller values of α is not difficult to write into the program.

3. The Convolution Integrals

Concerning selection of the basic time increment, it was found that $c\Delta t = \rho/400$ gave better than 1% accuracy for times up to $4\rho/c$ behind the diffracted wavefront. Using this incrementation, the expressions (53b) and (53c) are programmed in a subroutine AMPS(GRHO, GPHI) and returned to the main program evaluated at a set of points separated by the selected value of $c\Delta t$. The convolution of these functions with the similarly evaluated dipole moment function is carried out by the trapezoidal rule with three exceptions: (1) If the convolution extends over one time interval only, the dipole moment function is assumed to

vary quadratically, then the ρ and ϕ components of the Hertz potential for the impulsive source vary like $t^{1/2}$ and $t^{-1/2}$, respectively; and the integral is evaluated analytically in terms of the values of PNN, GRHO and GPAI at the end of the first interval. (2) For larger multiples of $c\Delta t$ the contribution of the first interval is evaluated by assuming quadratic variation of PNN and linear variation of GRHO and an GPHI. (3) The last interval contribution is evaluated assuming linear variation for PNN, $t^{1/2}$ for GRHO, and $t^{-1/2}$ for GPHI. These convolution integrals are stored, as arrays, for all 6 points necessary for numerical differentiation under the names PIRHO and PIPHI.

4. Numerical Differentiation

Numerical differentiation is straightforward, with one exception. Since the N^{th} value of PIRHO or PIPHI denotes the values of these potentials N time intervals behind the diffracted wavefront, a change in the ρ coordinate of the observation point involves both a change in the coordinates for which $\hat{G}_\rho$, $\hat{G}_\varphi$ are evaluated (i.e. a different value of J from among the 6 points) and an appropriately different value of N for absolute (i.e. not "behind wavefront") time. Hence, differentiation with respect to ρ involves simultaneous shifts in both J and N. For simplicity $\Delta\rho = c\Delta t$ was used, so that the appropriate shift in N is unity. The differentiation was carried out numerically according to (56) - (58).

5. Geometric Optical Fields

The geometric optical field consists of the incident and reflected fields. The latter can be evaluated by the method of images, taking into account the time delays between the times of arrival of the various field constituents and restricting appropriately the angular range of contribution. These computations are included in a subroutine labelled GEOFD, for which another subroutine, DIPFLD, is provided for evaluating the radiation from a dipole in free space.

6. Normalization

The normalization in this computer program was intended to facilitate comparison with the results of Baum [1] and Higgins [2]. The electric and magnetic fields are normalized to the discontinuities in the incident fields at the wavefront when the latter is at the edge of the wedge. Time is printed out in units of ρ/c and $t = 0$ corresponds to the time of arrival of the incident wave at the observation point.

References

1. C. E. Baum, "The Diffraction of an Electromagnetic Plane Wave at a Bend in a Perfectly Conducting Planar Sheet", Sensor and Simulation Note 47, August 1967.

2. D. F. Higgins, "The Diffraction of an Electromagnetic Plane Wave by Interior and Exterior Bends in a Perfectly Conducting Sheet", Sensor and Simulation Note 128, Jan. 1971.

3. F. Oberhettinger, "On the Diffraction and Reflection of Waves and Pulses by Wedges and Corners", J. Res. Nat. Bur. Standards 61 (1958), p. 343-365.

4. A. Mohsen and T. B. A. Senior, " The Impulse Response of a Half Plane", IEEE Transactions on Antennas and Propagation, AP-21 (1973), p. 254-255.

5. J. A. Stratton, "Electromagnetic Theory", McGraw-Hill, New York (1941) Sec. 1.11.

6. G. D. Malyuzhinets and A. A. Tuzhilin, "The Electromagnetic Field Excited by an Electric Dipole in a Wedge-Shaped Region", Soviet Physics - Doklady 7 (1963), p. 879-882.

7. L. B. Felsen and N. Marcuvitz, "Radiation and Scattering of Waves", Prentice-Hall, Inc., Englewood Cliffs, New Jersey (1973), Secs. 5.2c and 6.5.

8. E. T. Whittaker and G. N. Watson, "A Course of Modern Analysis", Cambridge University Press (1952), p. 123.

9. C. E. Baum, "Some Characteristics of Electric and Magnetic Dipole Antennas for Radiating Transient Pulses", Sensor and Simulation Note 125, Jan. 1971.

10. D.S. Jones, "The Theory of Electromagnetism", McMillan Co., New York (1964), p. 152.

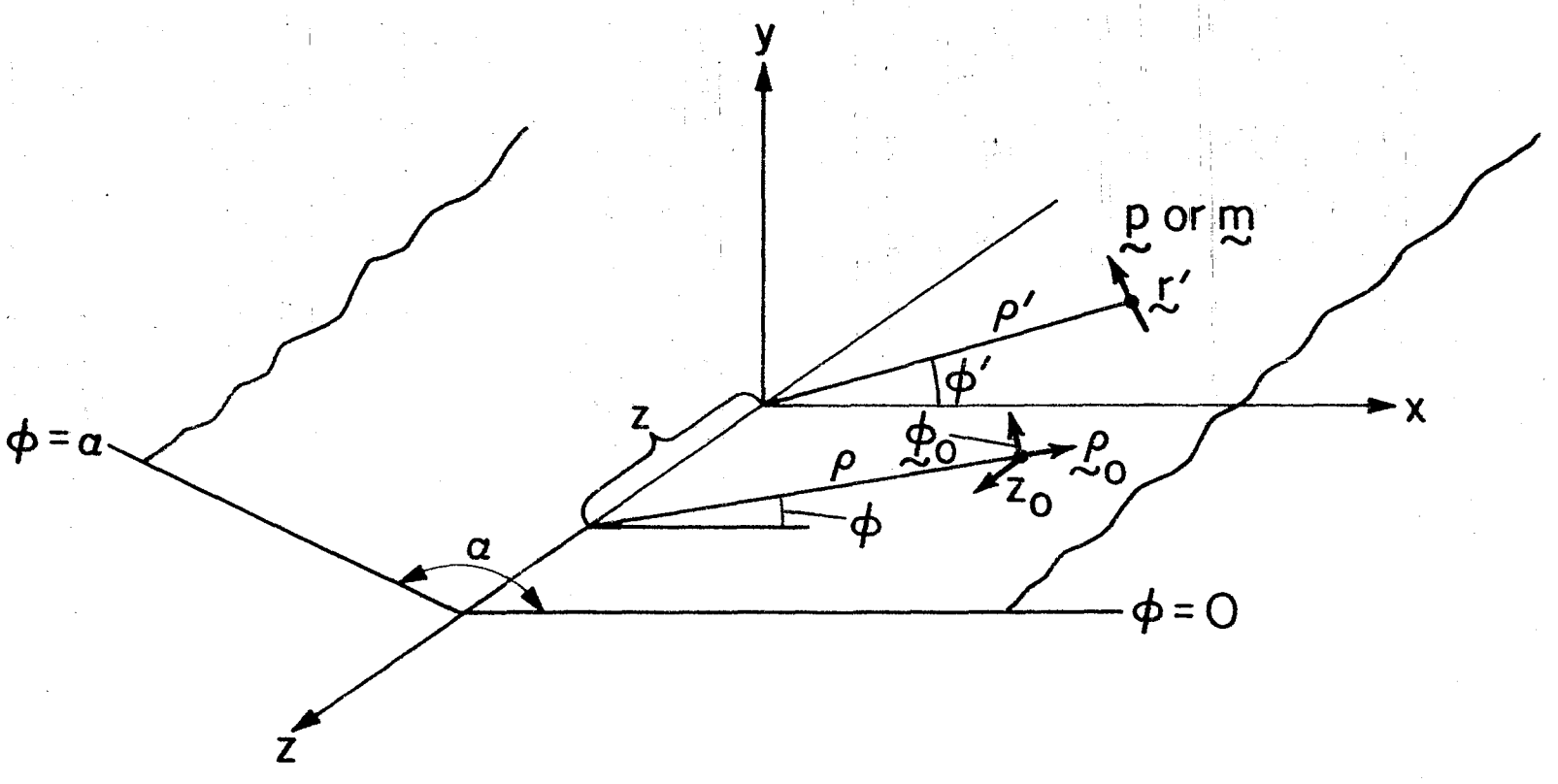

Fig. 1 Wedge Configuration

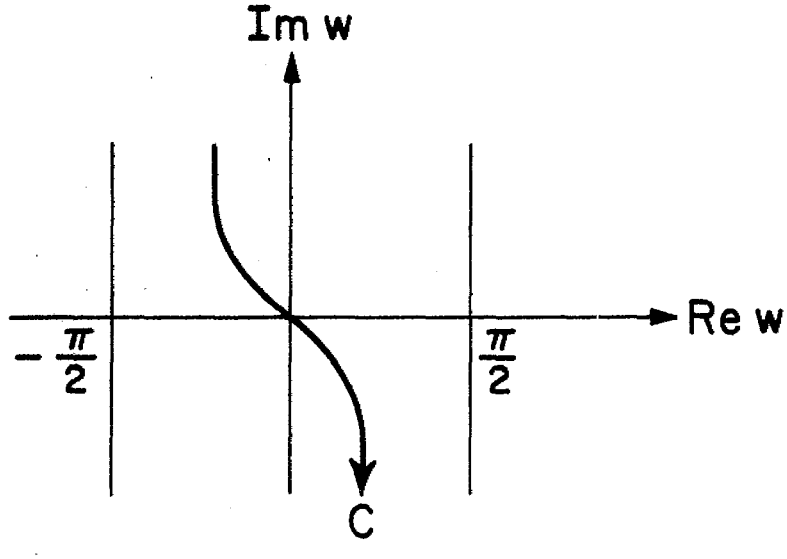

Fig. 2 Integration Path in Complex w-plane

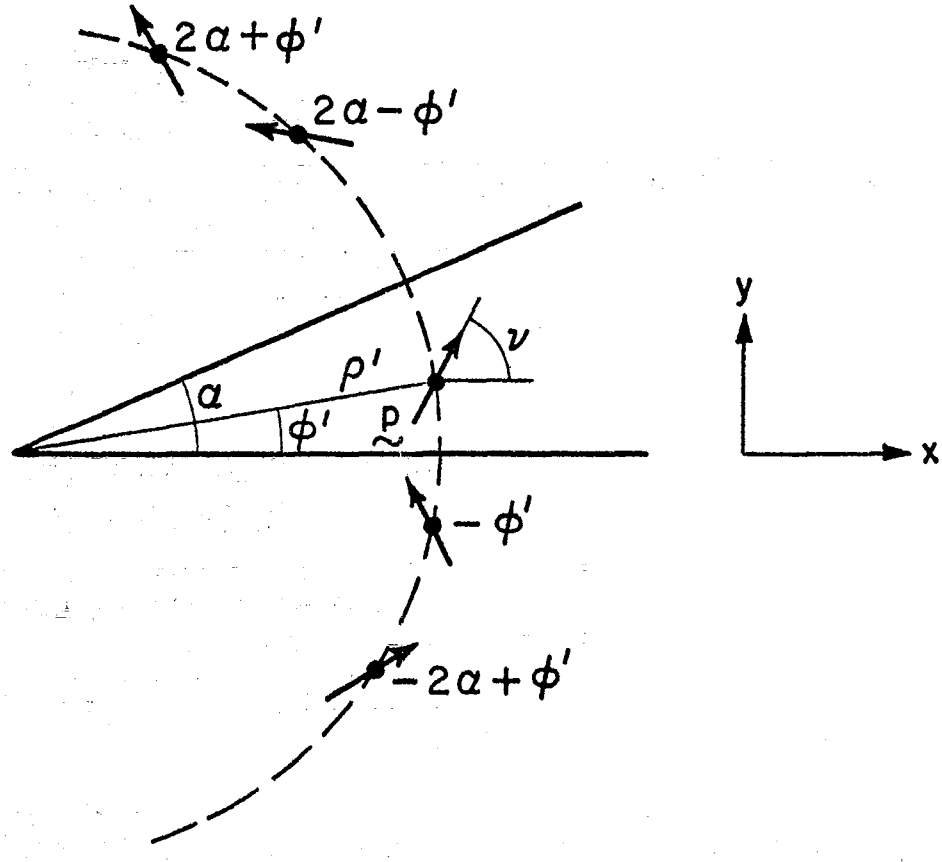

Fig. 3 Image Configuration

PULSE SHAPE REQUIRED TO PRODUCE STEP FIELD

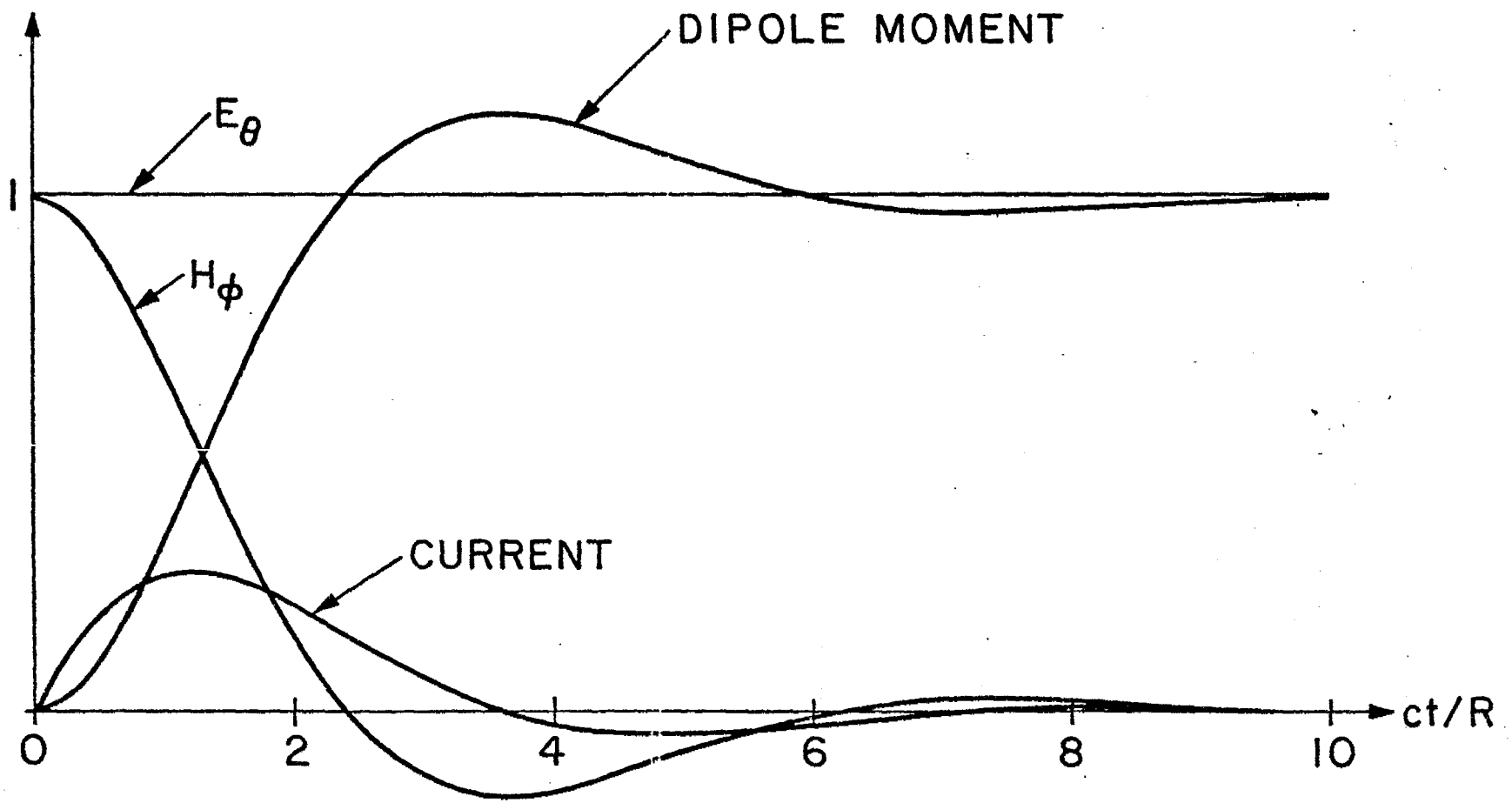

Fig. 4 Pulse Shape Required to Produce Step Field

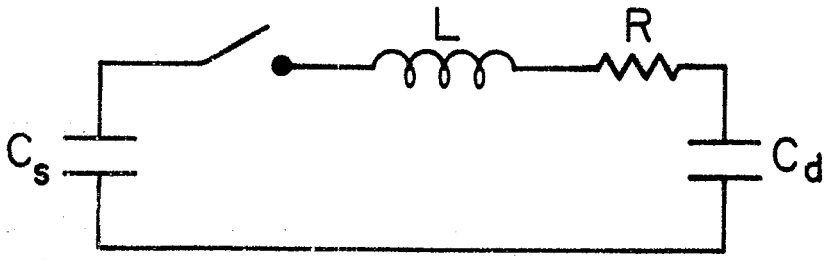

Fig. 5 Pulse Forming Circuit

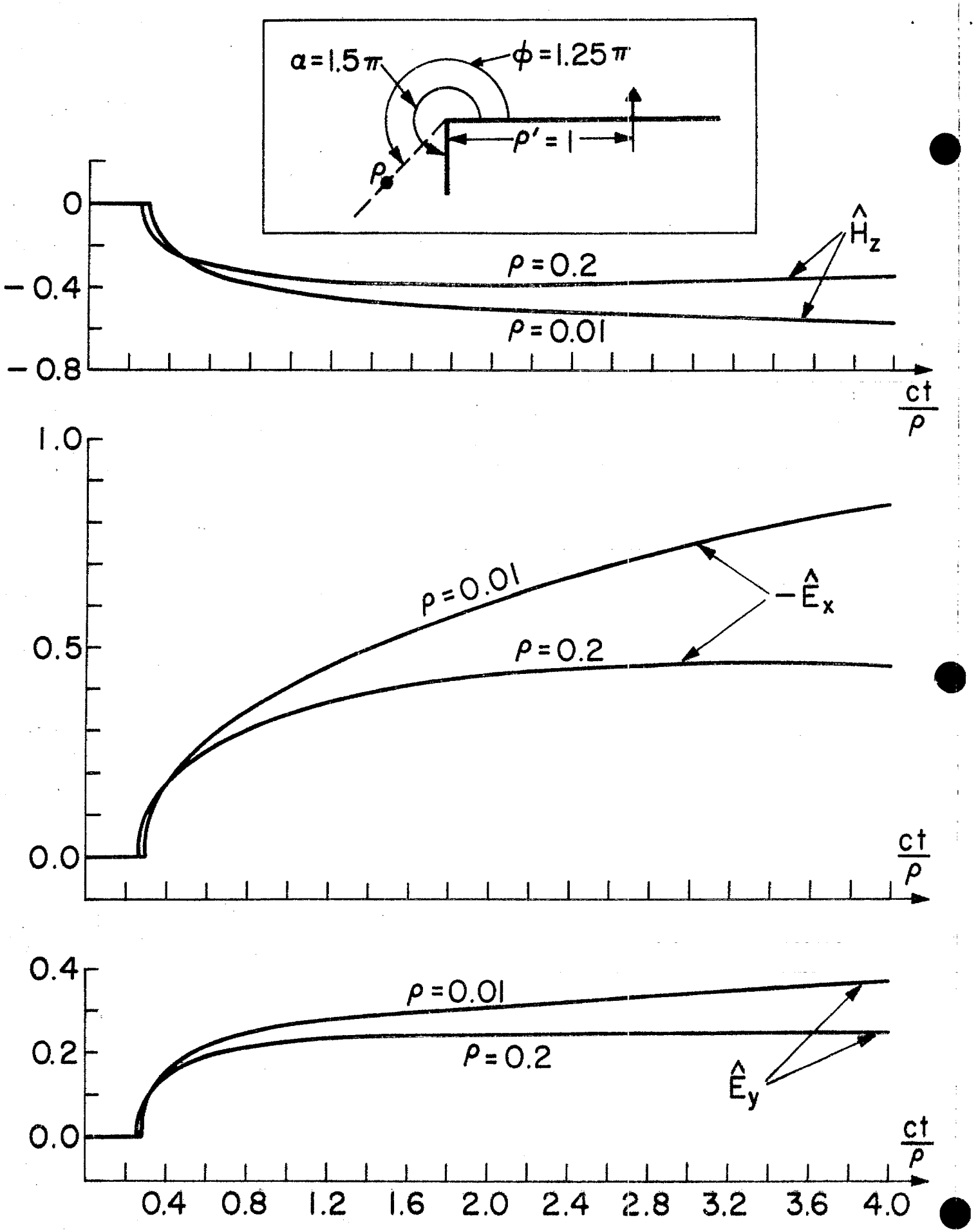

Fig. 6(a) Field Calculation: Diffracted Wave Only

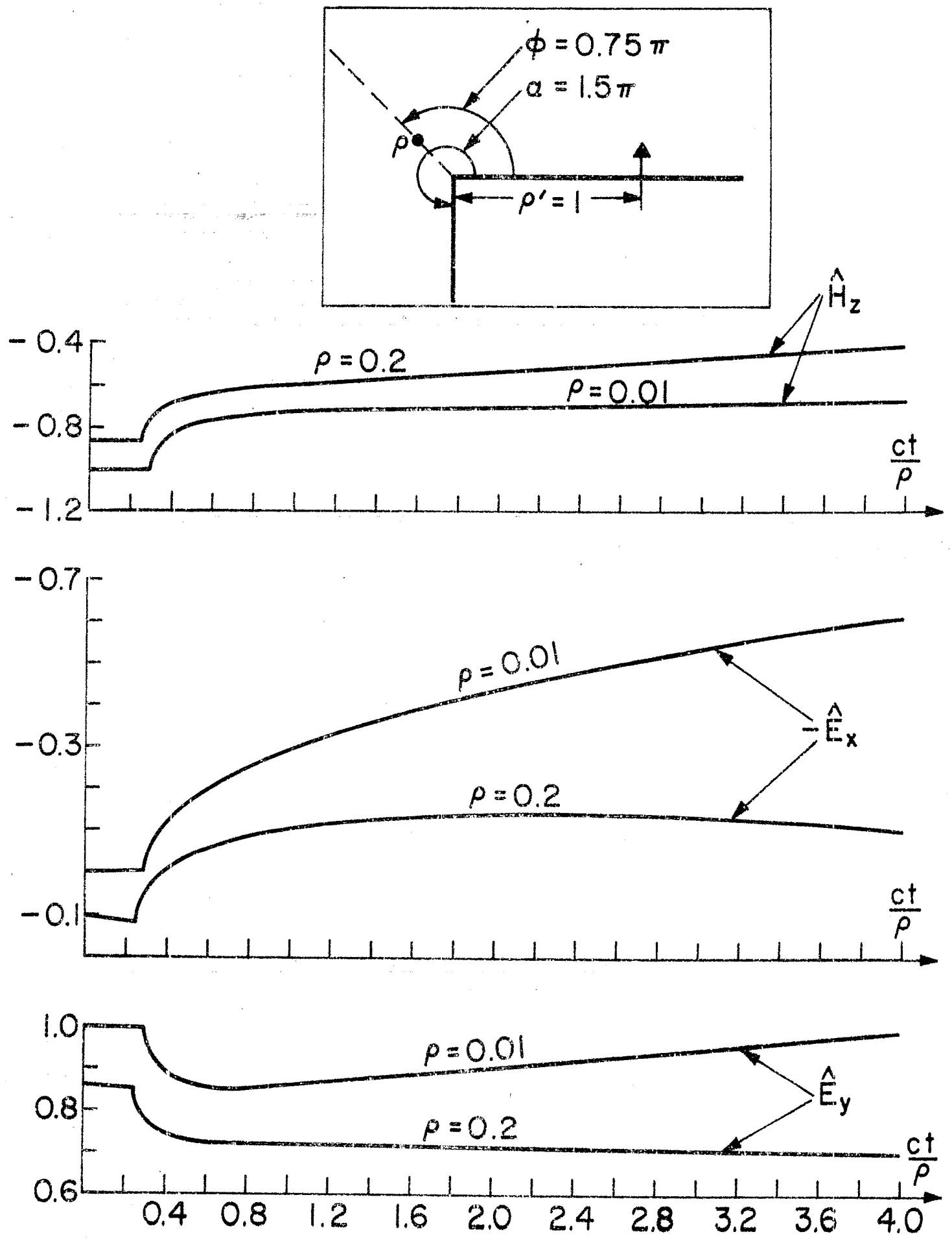

Fig. 6(b) Field Calculation: Incident and Diffracted Waves

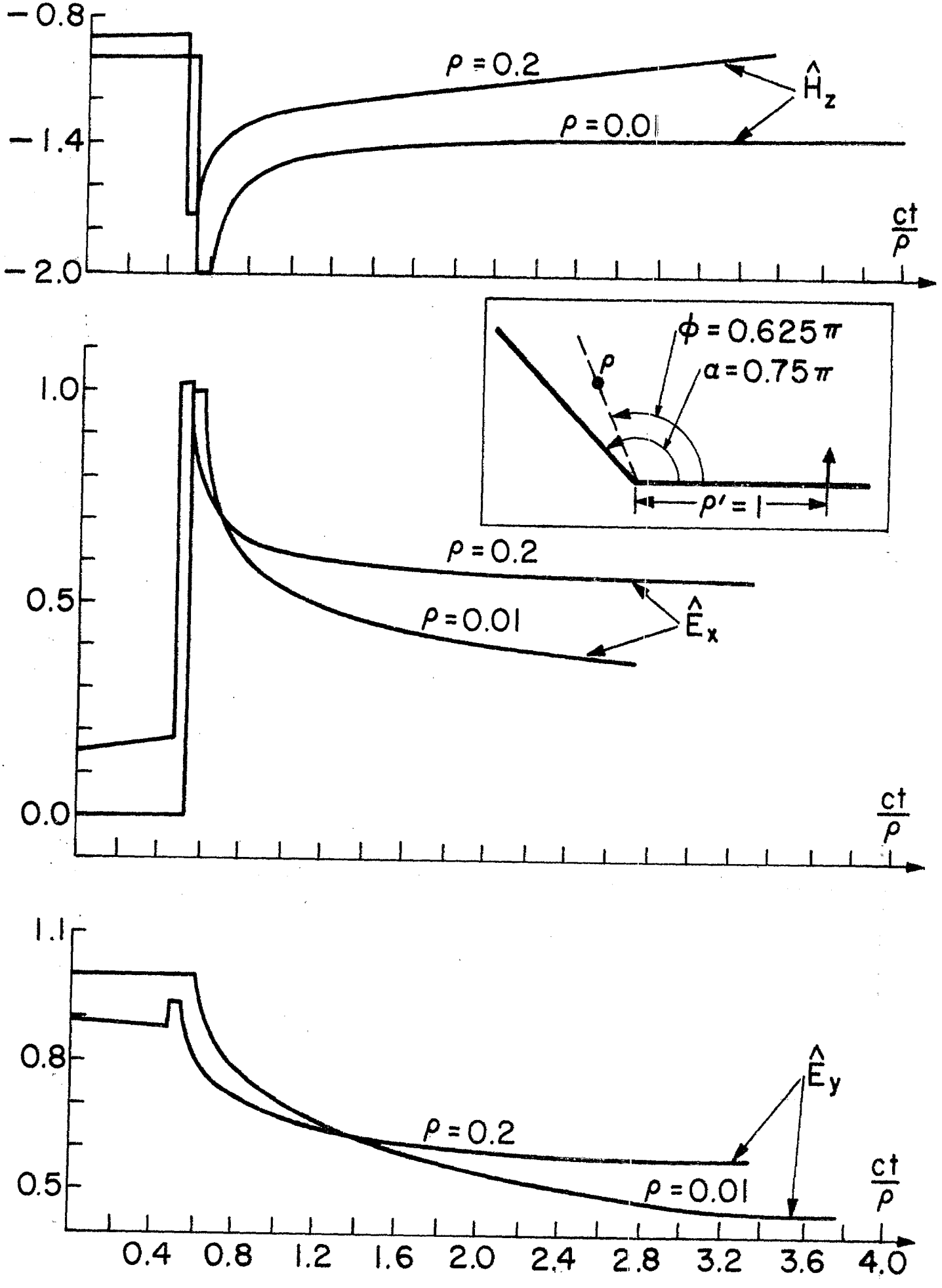

Fig. 6(c) Field Calculation; Incident, Reflected and Diffracted Waves

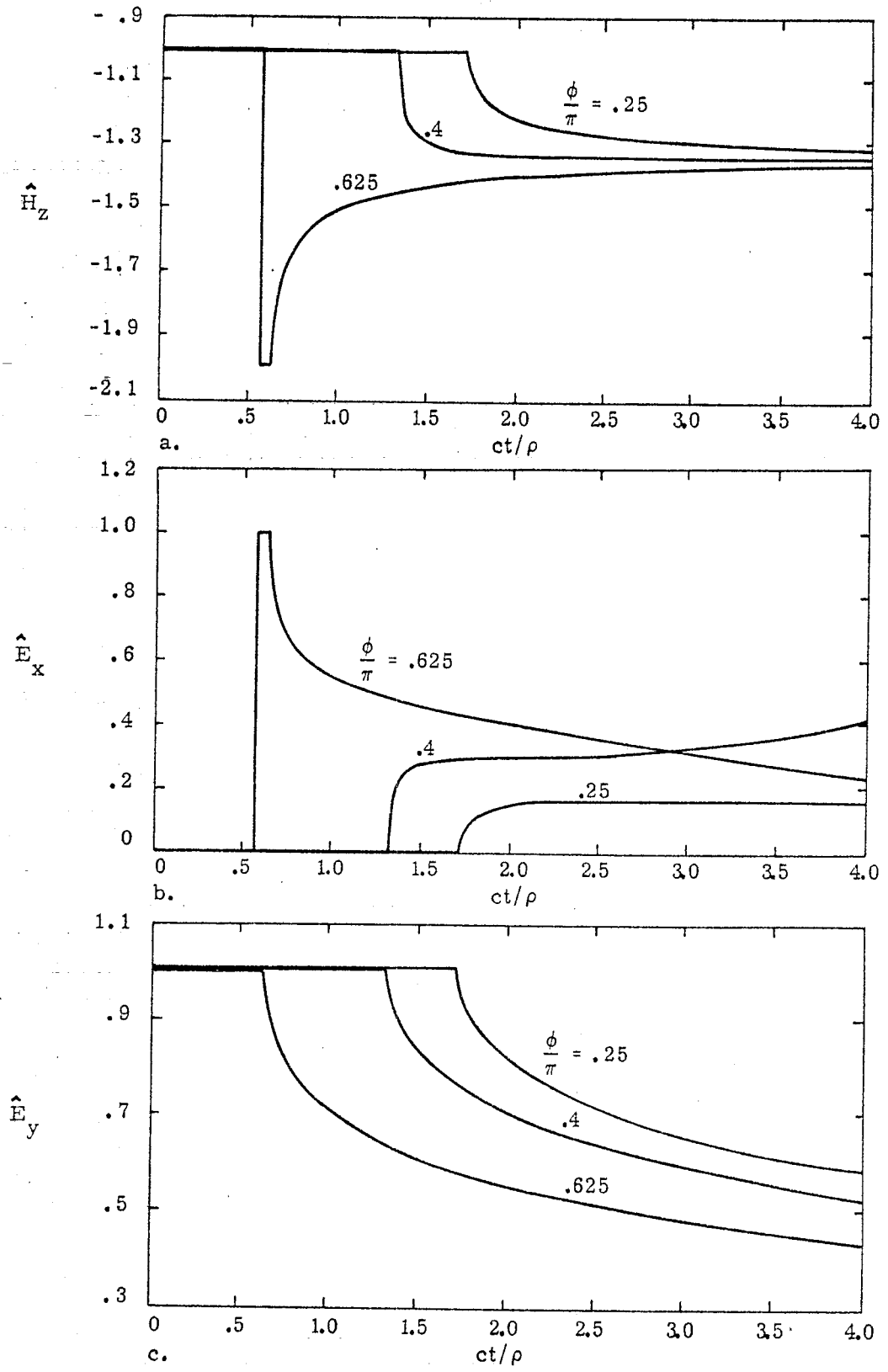

Figure 7. Field Calculation: $\rho = 0.01$, $\alpha = 0.75\pi$

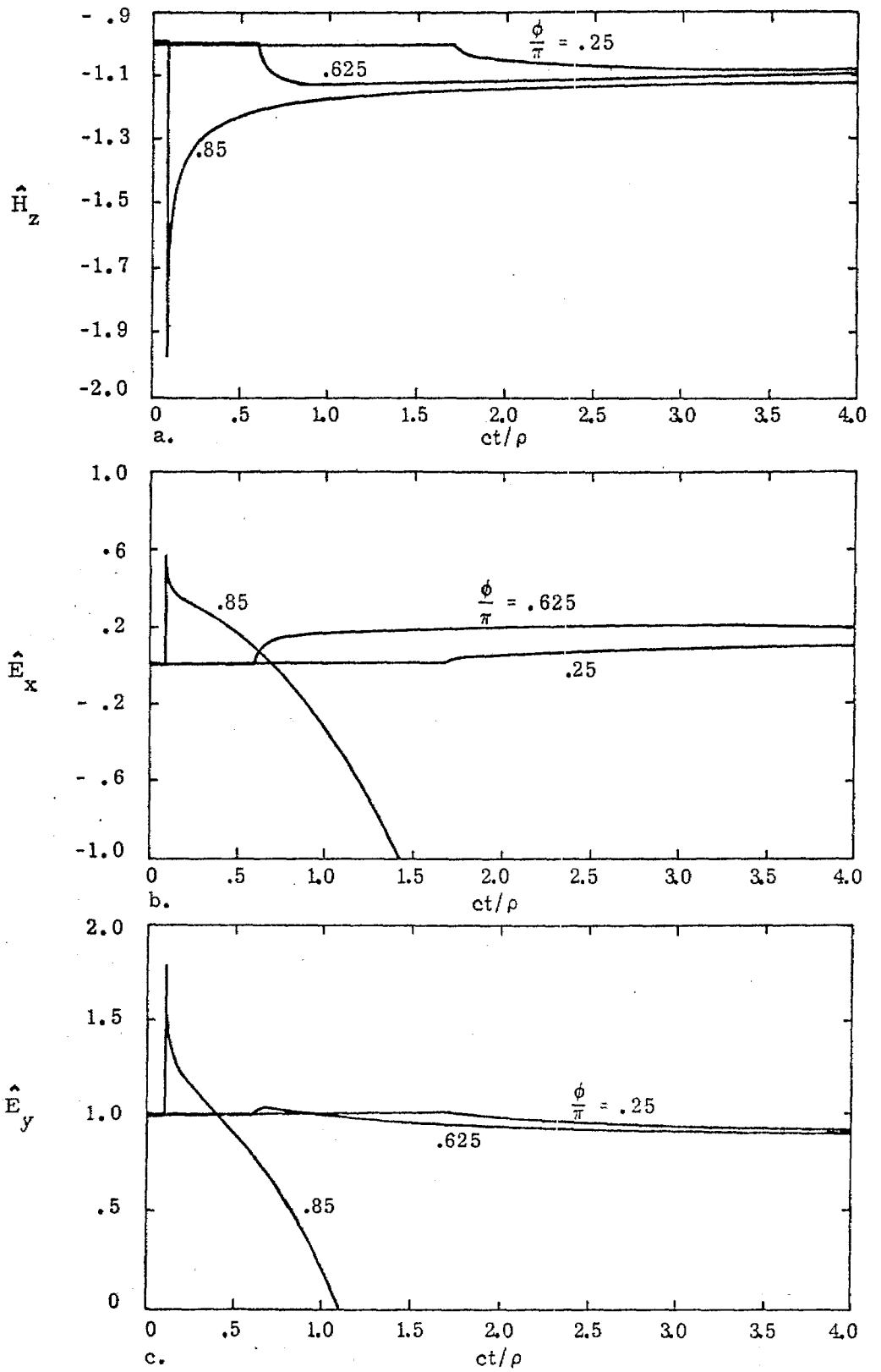

Figure 8. Field Calculation: $\rho = 0.01$, $\alpha = 0.9\pi$

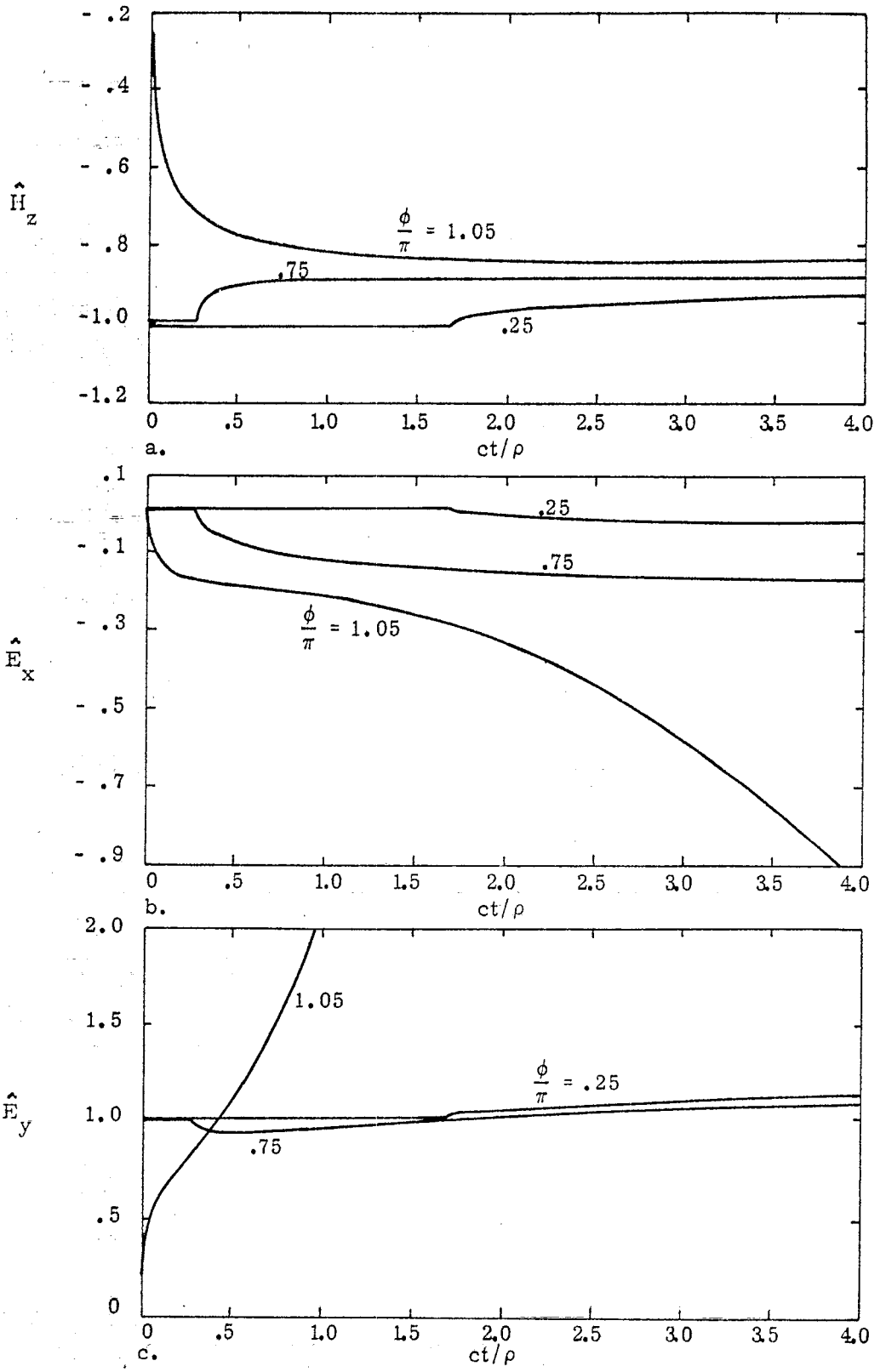

Figure 9. Field Calculation: $\rho = 0.01$, $\alpha = 1.1\pi$

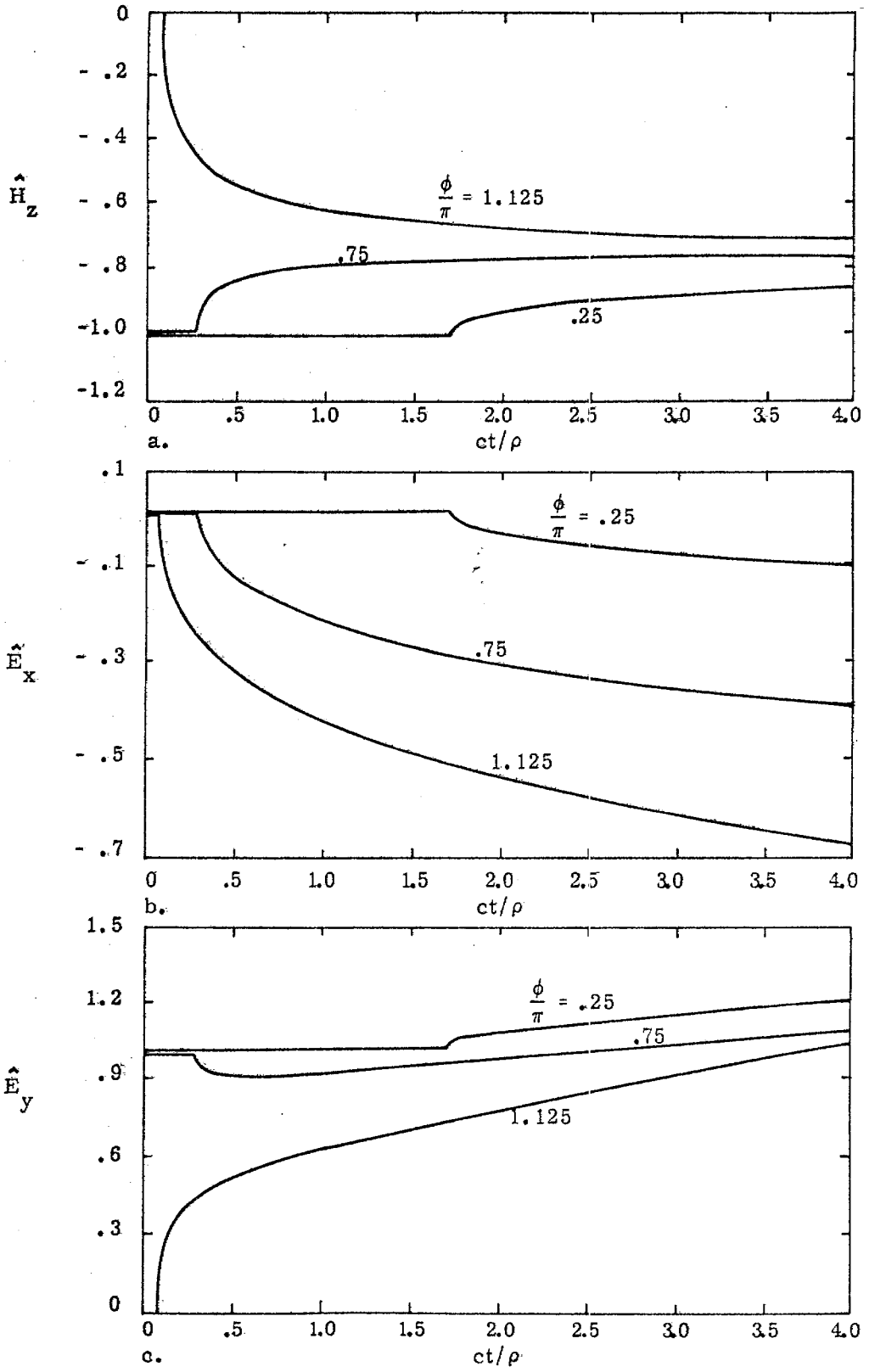

Figure 10. Field Calculation: $\rho = 0.01$, $\alpha = 1.25\pi$

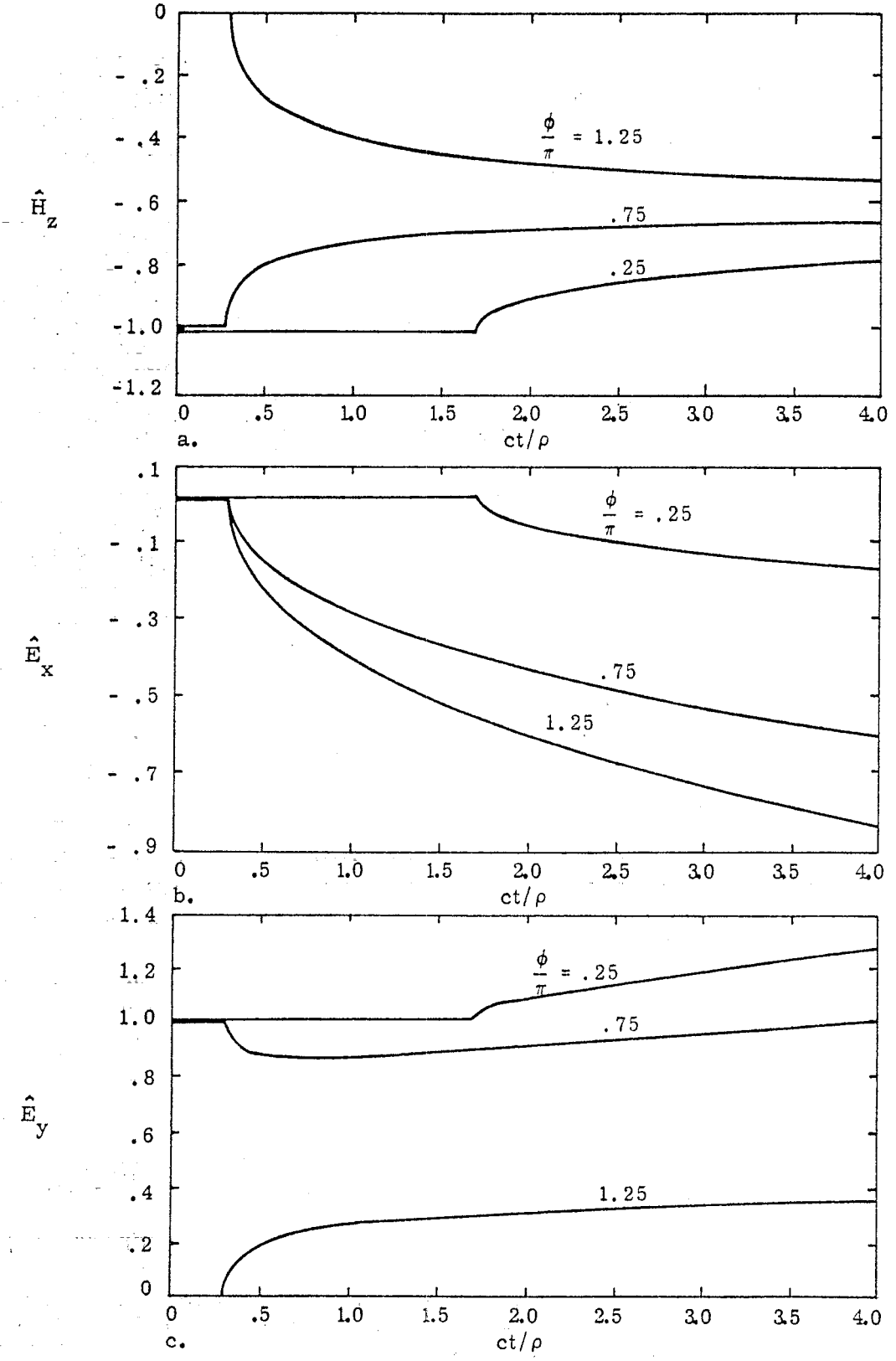

Figure 11. Field Calculation: $\rho = 0.01$, $\alpha = 1.5\pi$

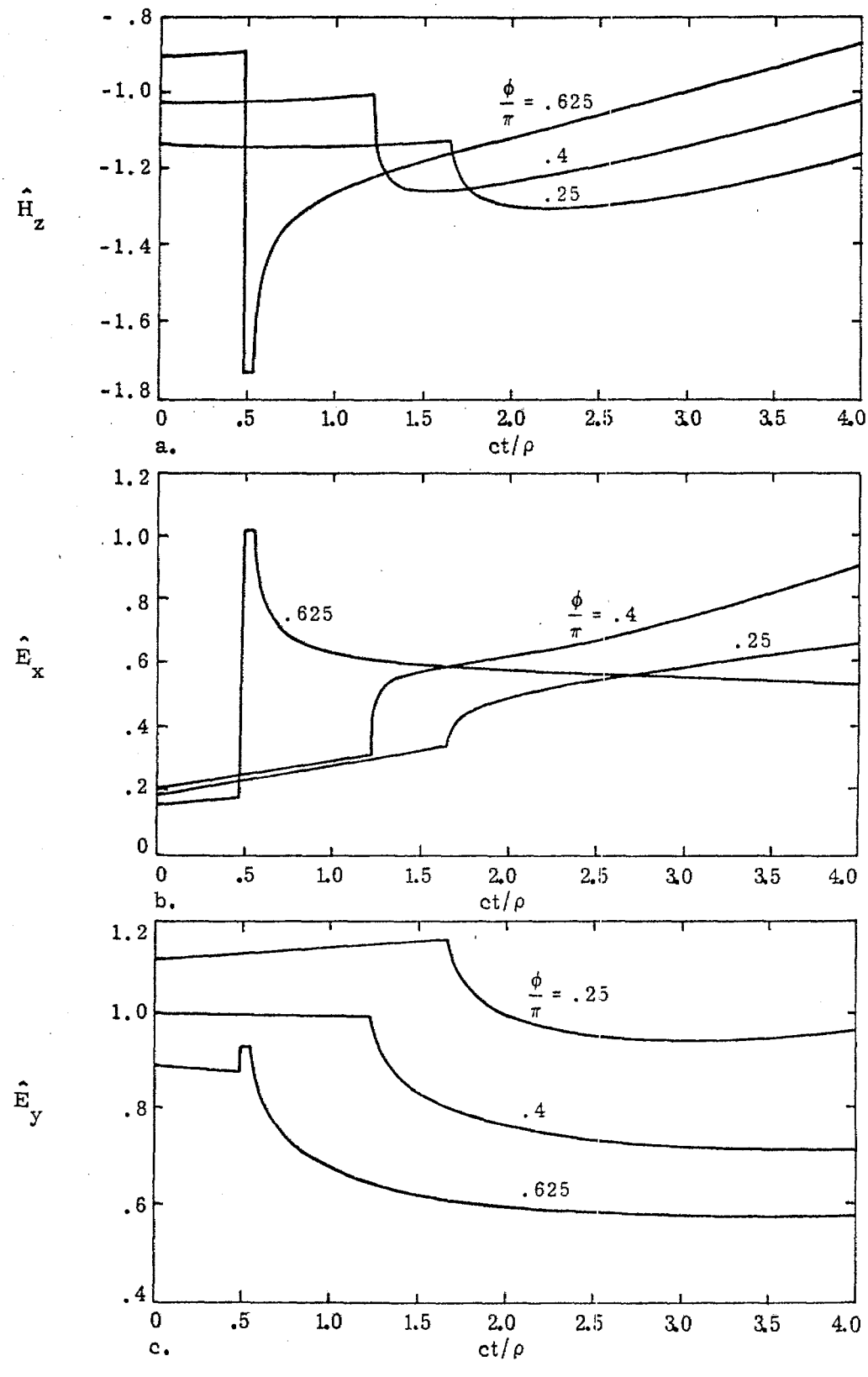

Figure 12. Field Calculation: $\rho = 0.2$, $\alpha = 0.75\pi$

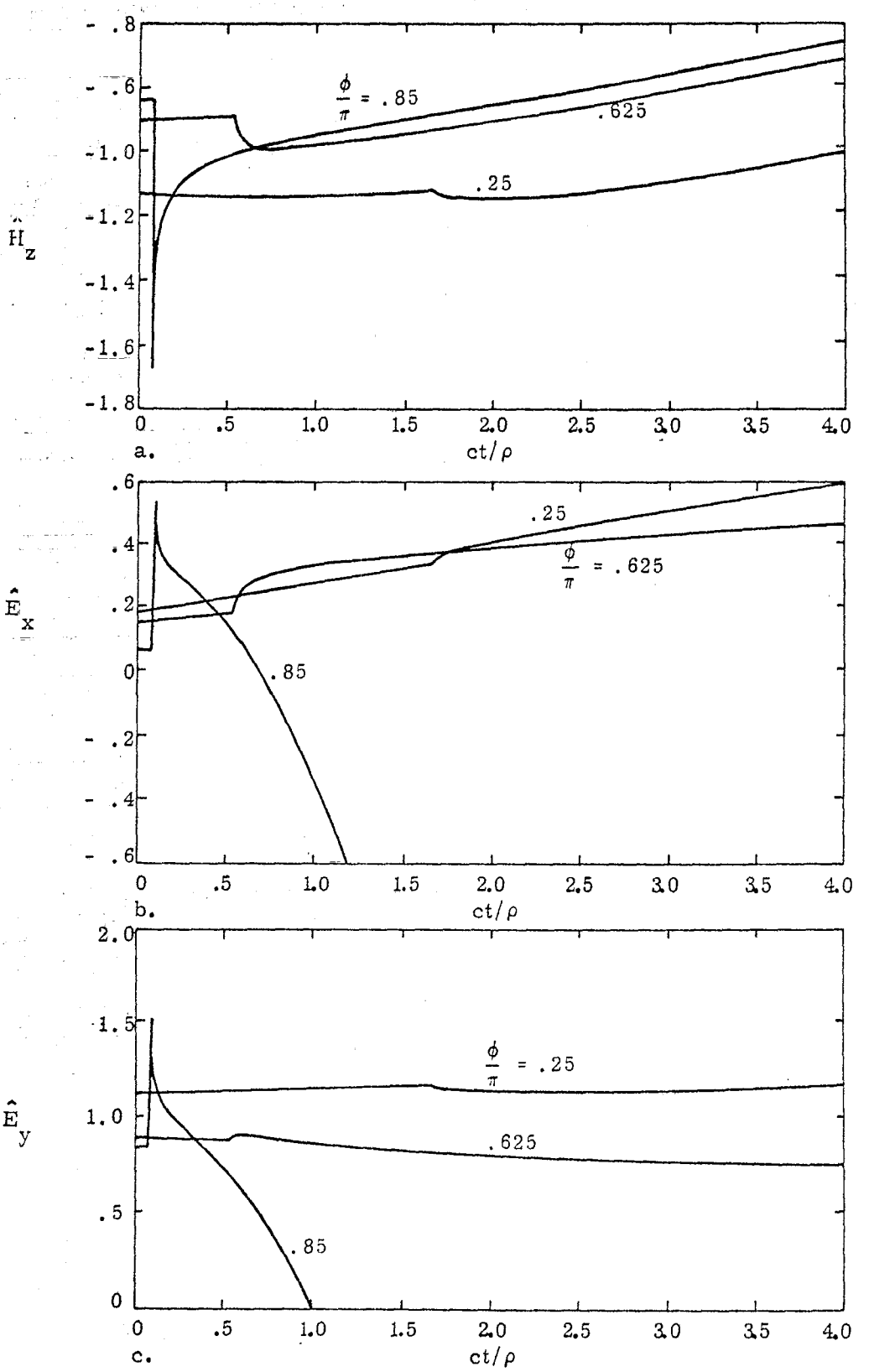

Figure 13. Field Calculation: $\rho = 0.2$, $\alpha = 0.9\pi$

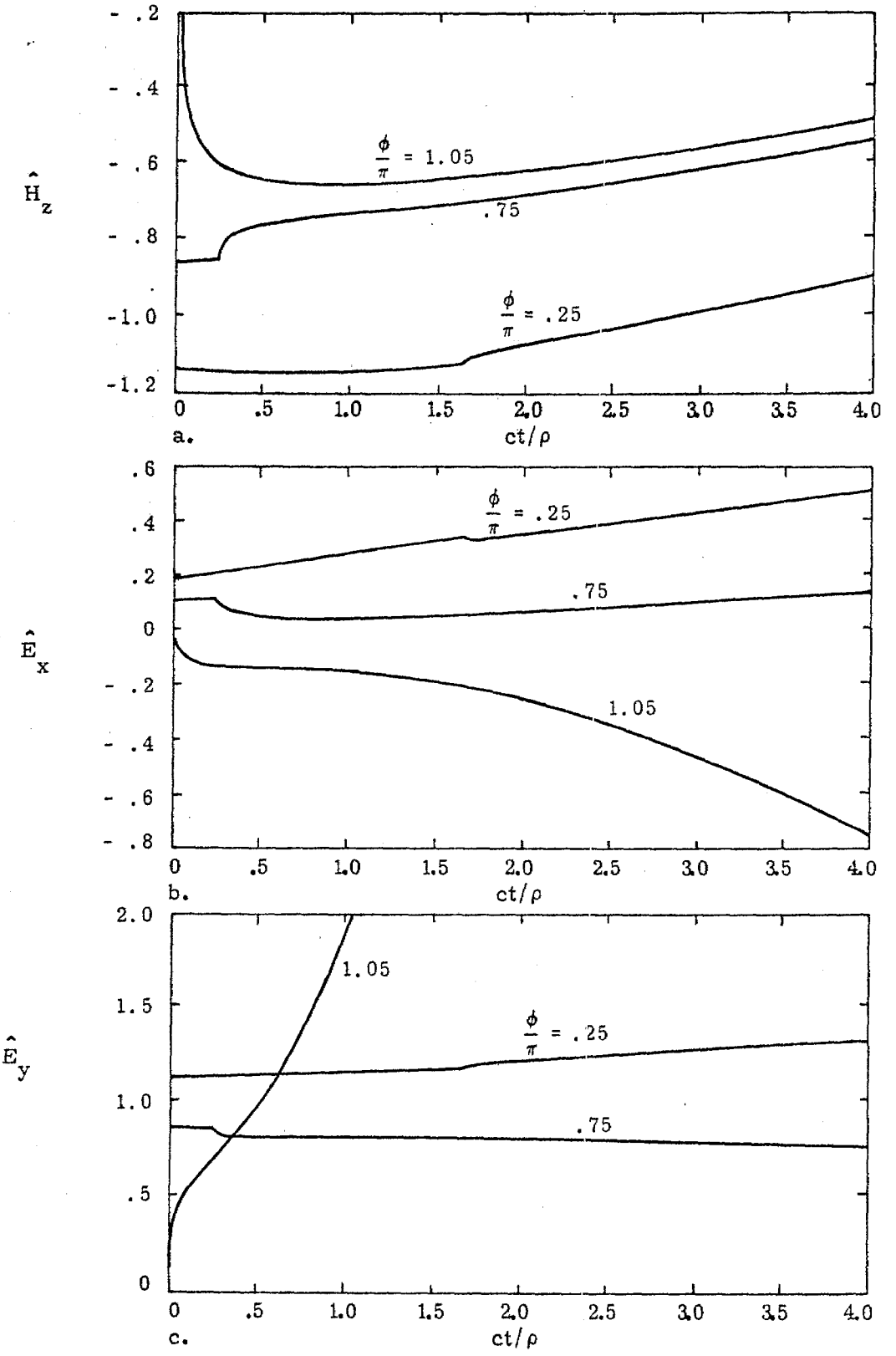

Figure 14. Field Calculation: $\rho = 0.2$, $\alpha = 1.1\pi$

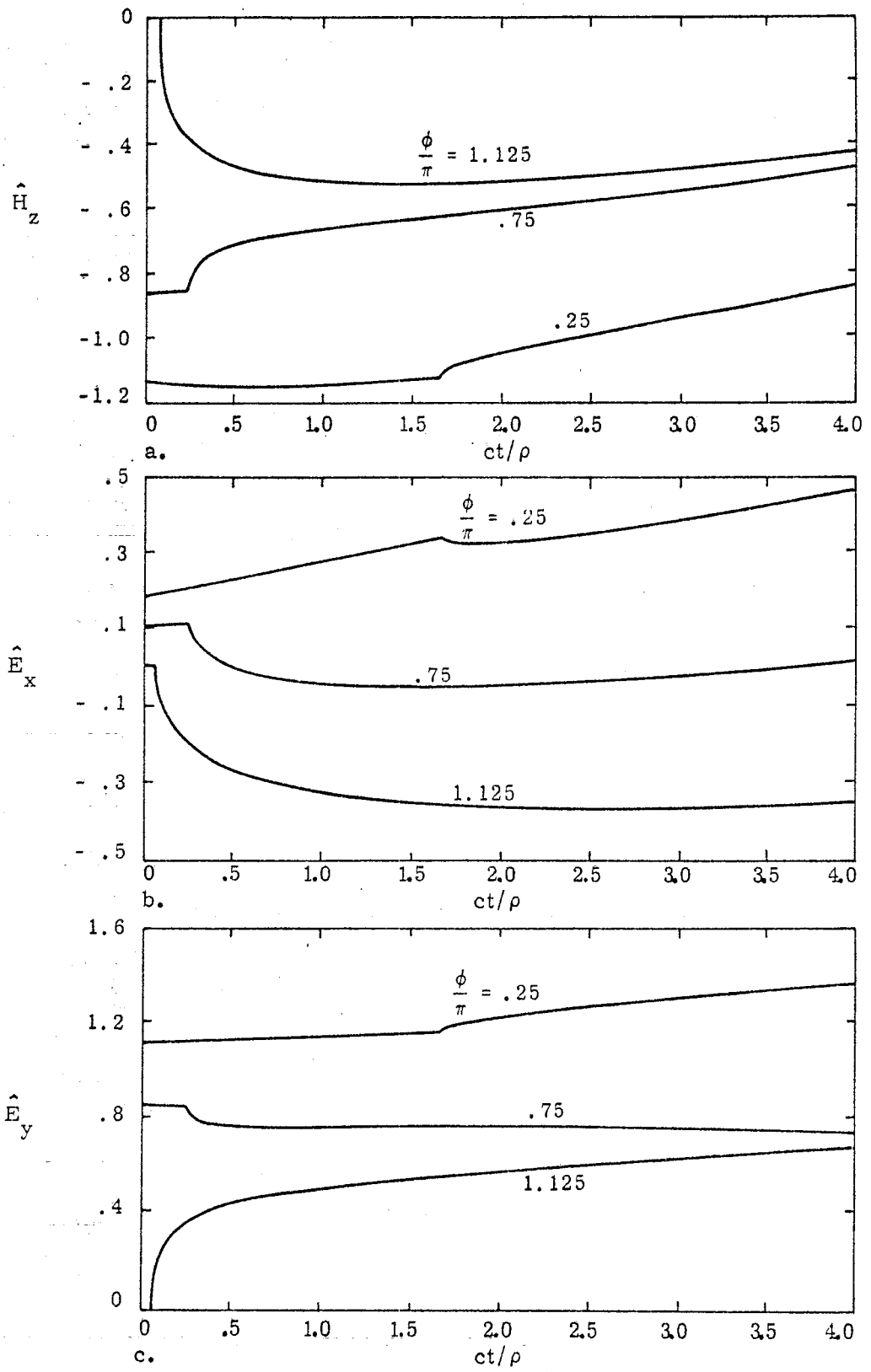

Figure 15. Field Calculation: $\rho = 0.2$, $\alpha = 1.25\pi$

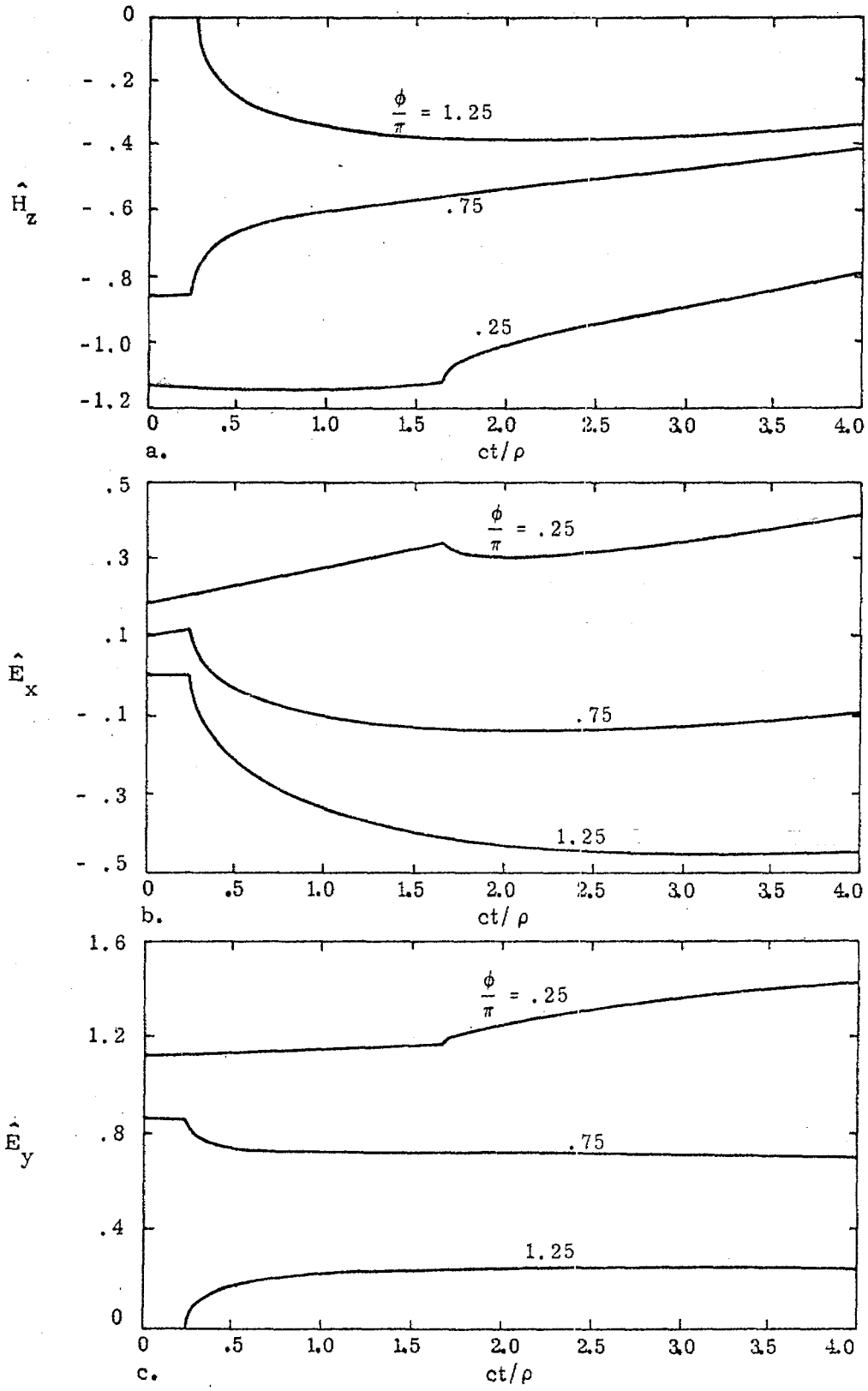

Figure 16. Field Calculation: $\rho = 0.2$, $\alpha = 1.5\pi$

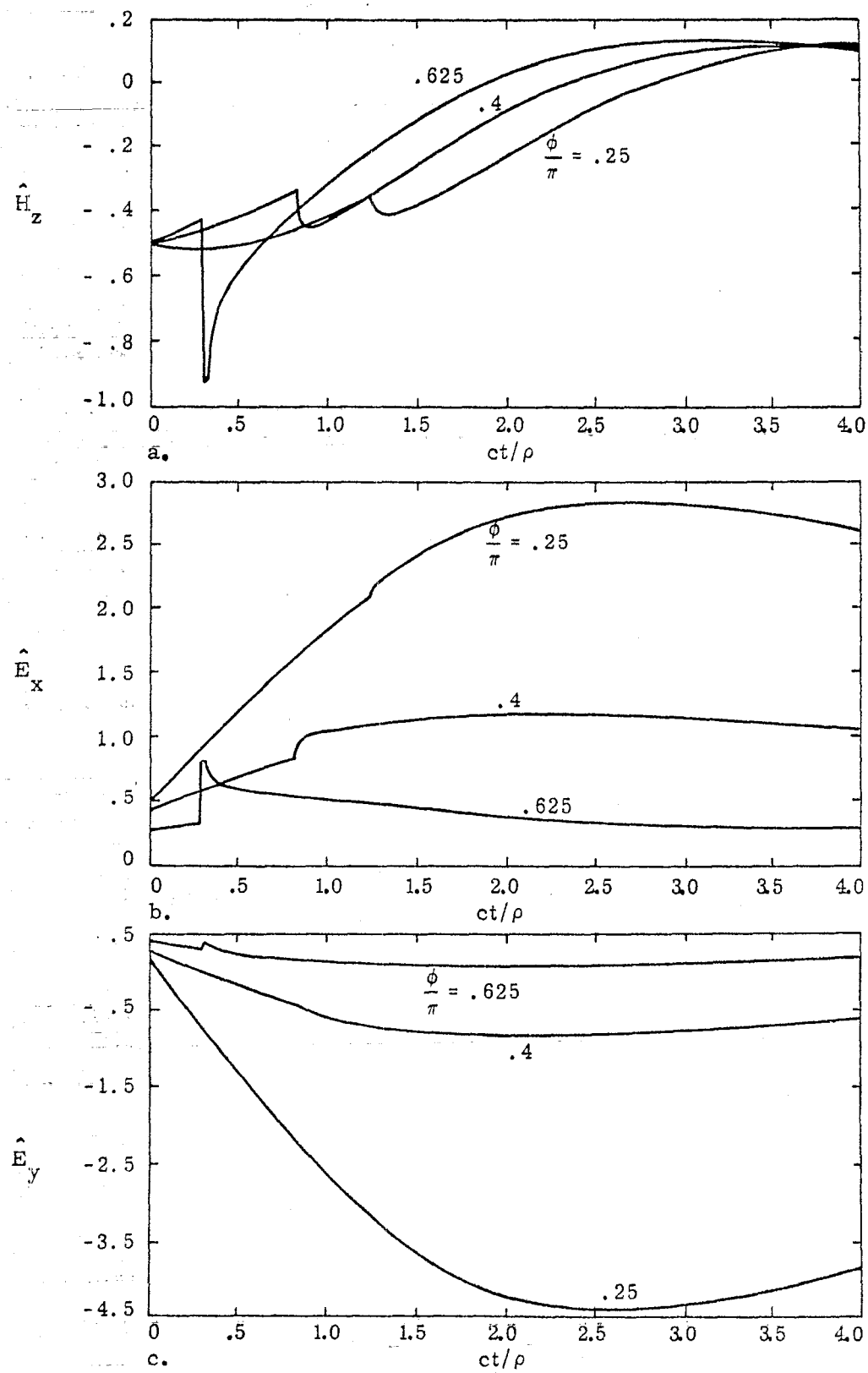

Figure 17. Field Calculation: $\rho = 1.0$, $\alpha = 0.75\pi$

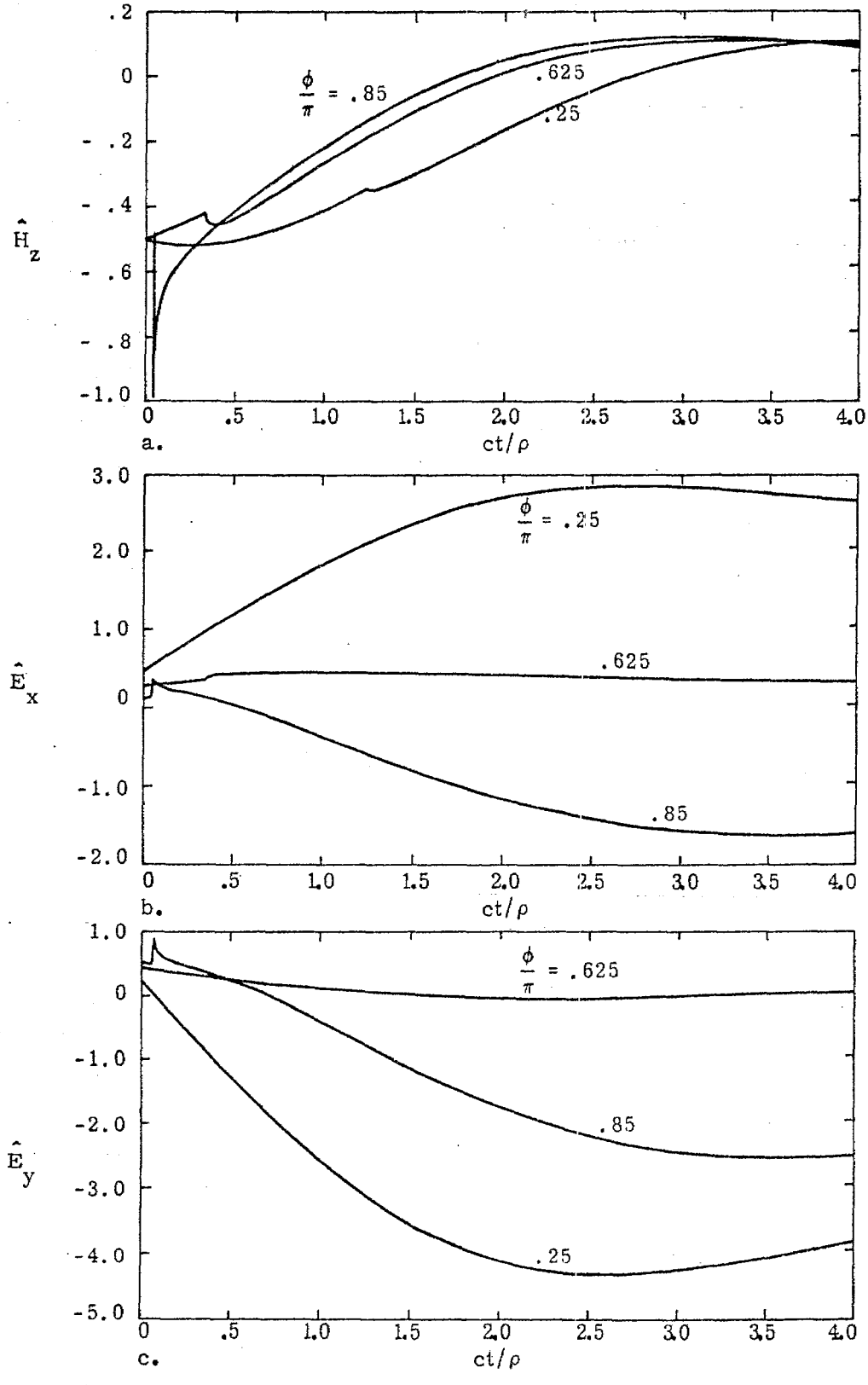

Figure 18. Field Calculation: $\rho = 1.0$, $\alpha = 0.9\pi$

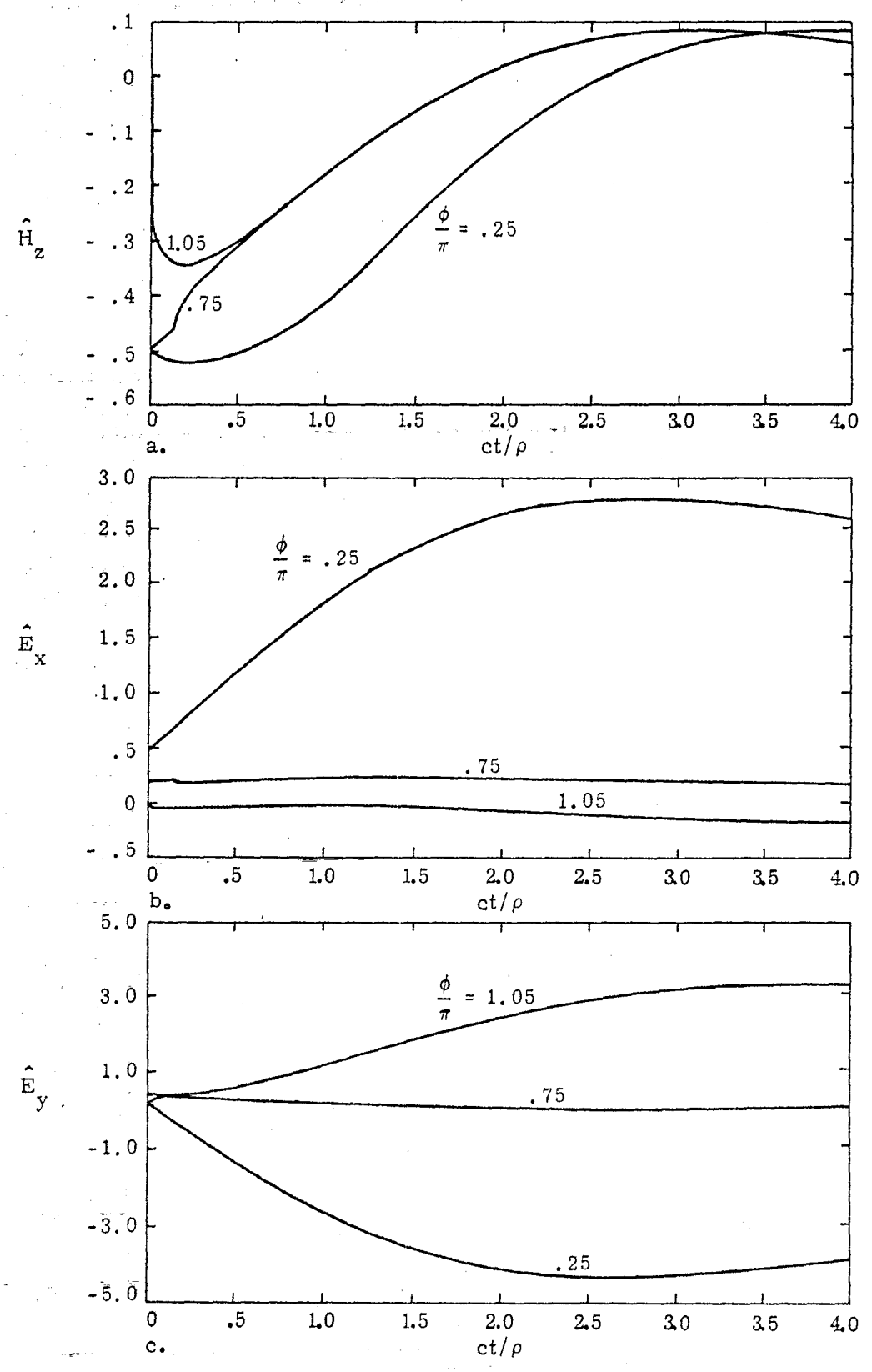

Figure 19. Field Calculation: $\rho = 1.0$, $\alpha = 1.1\pi$

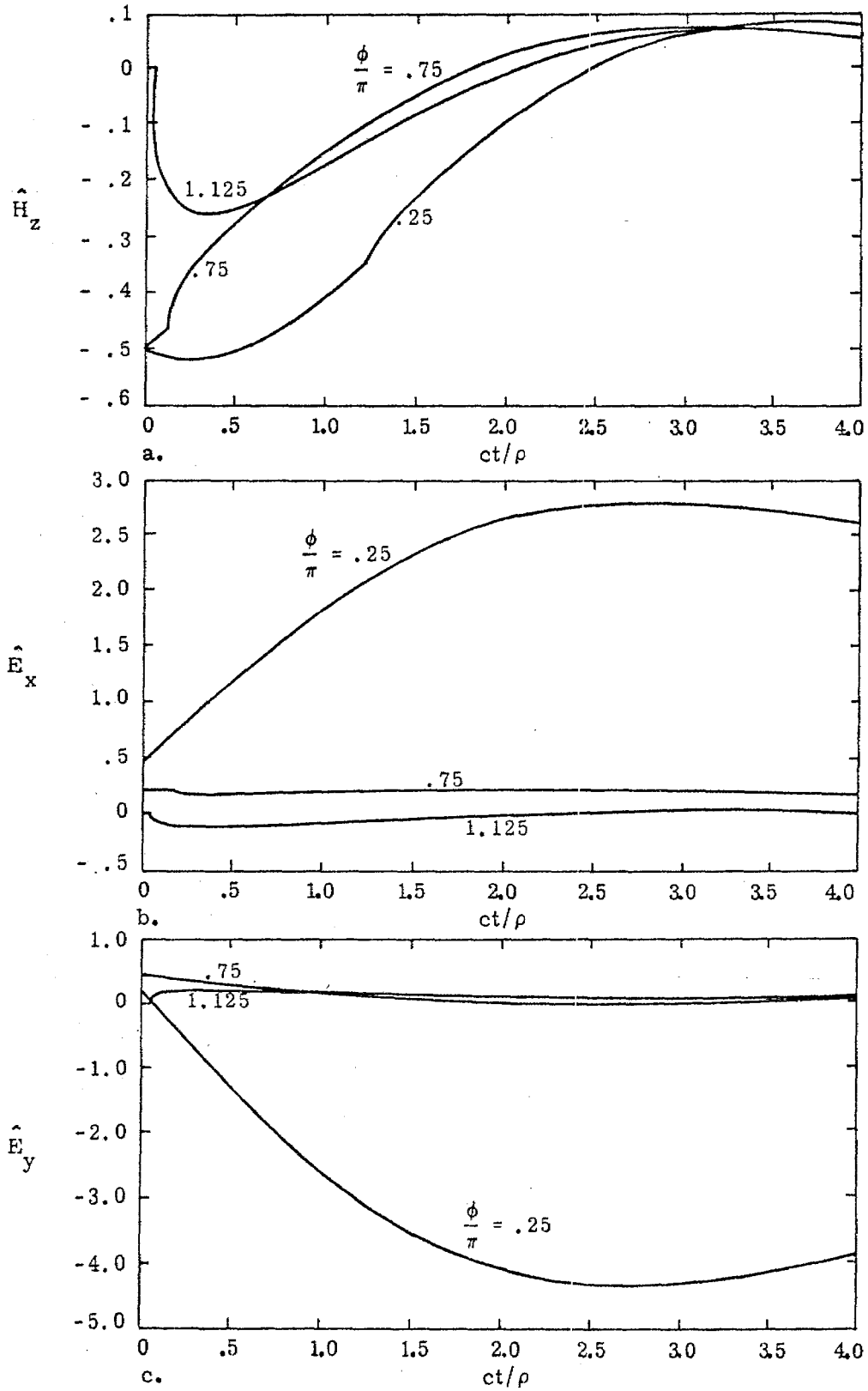

Figure 20. Field Calculation: $\rho = 1.0$, $\alpha = 1.25\pi$

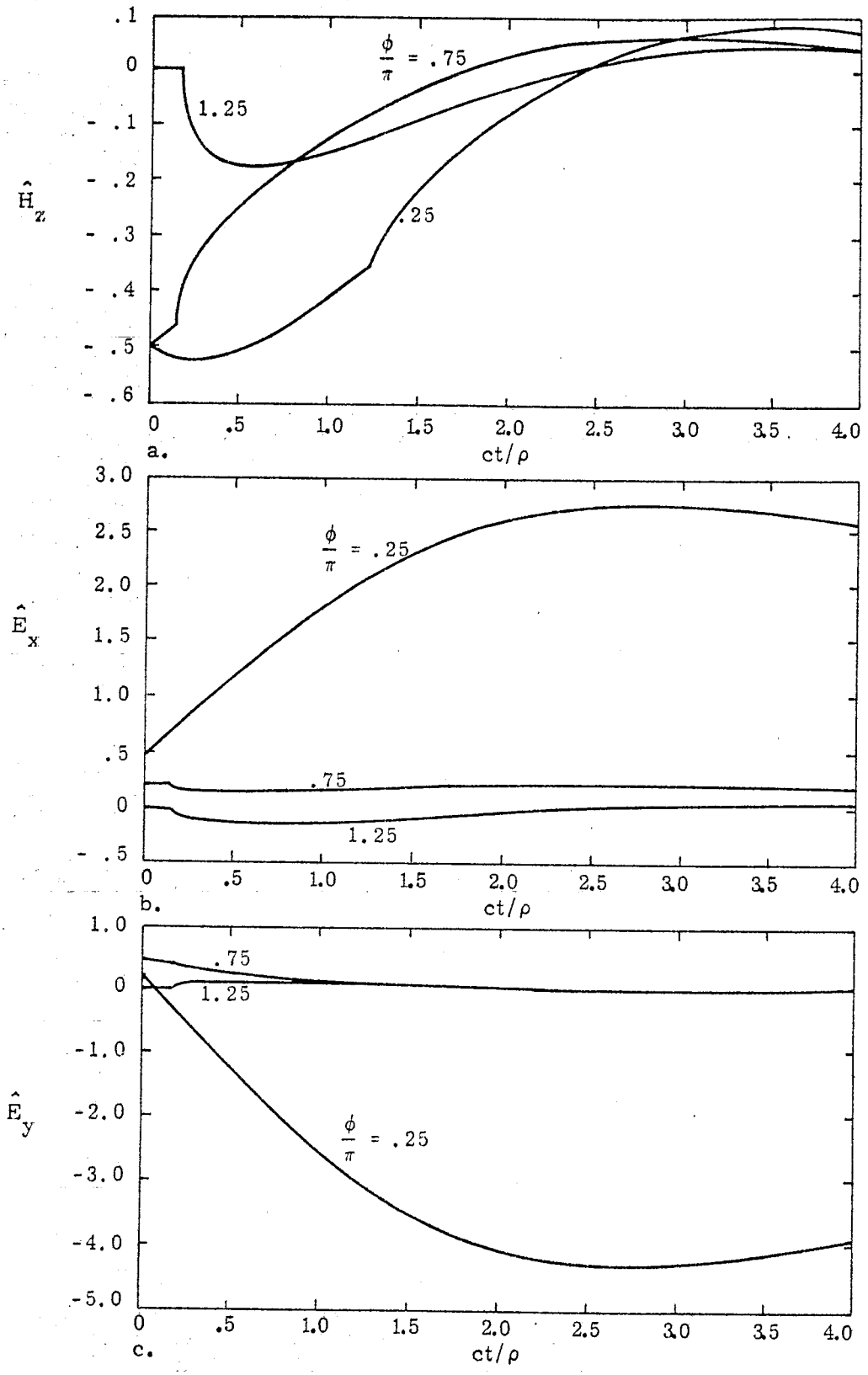

Figure 21. Field Calculation: $\rho = 1.0$, $\alpha = 1.5\pi$

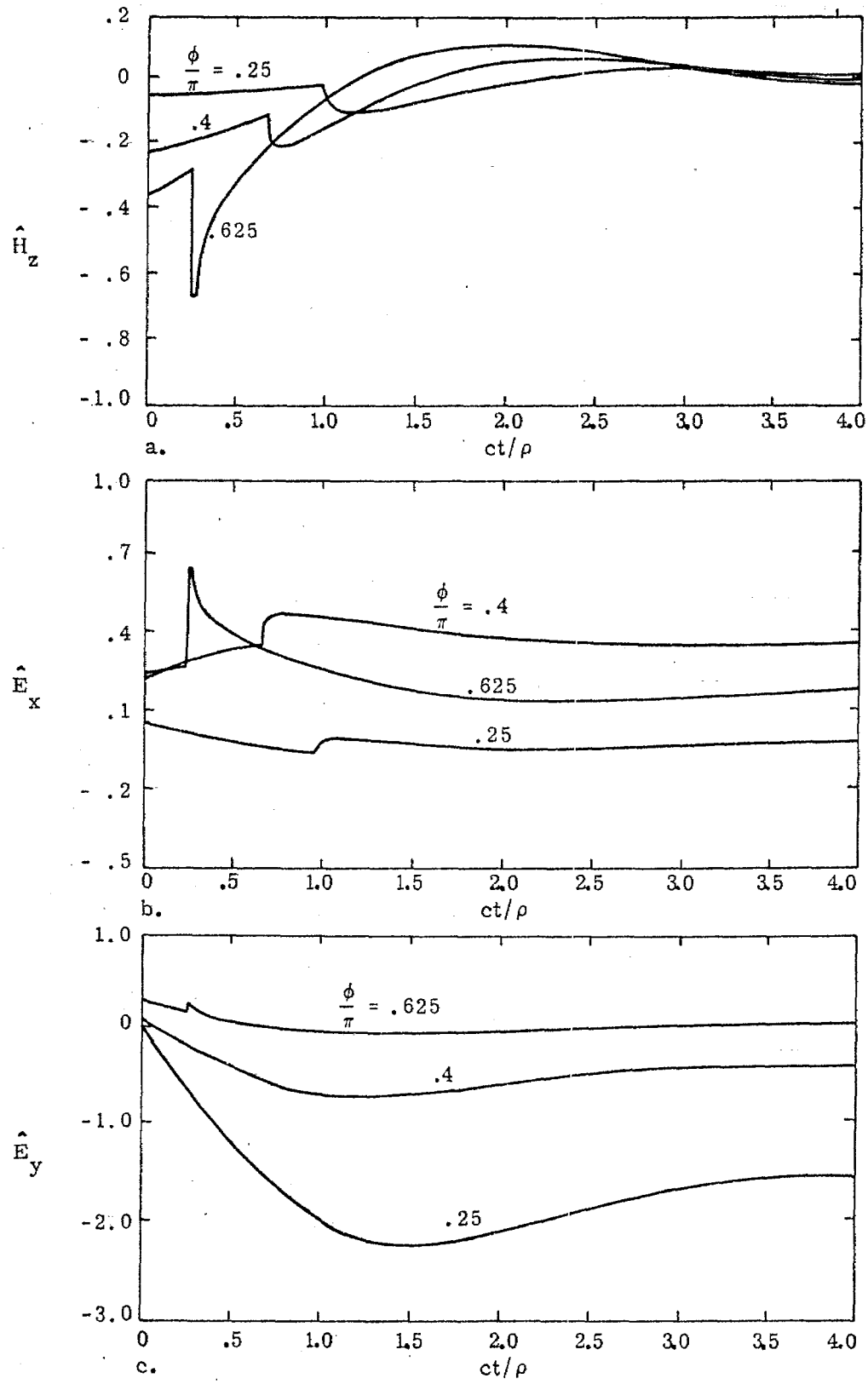

Figure 22. Field Calculation: $\rho = 1.5$, $\alpha = 0.75\pi$

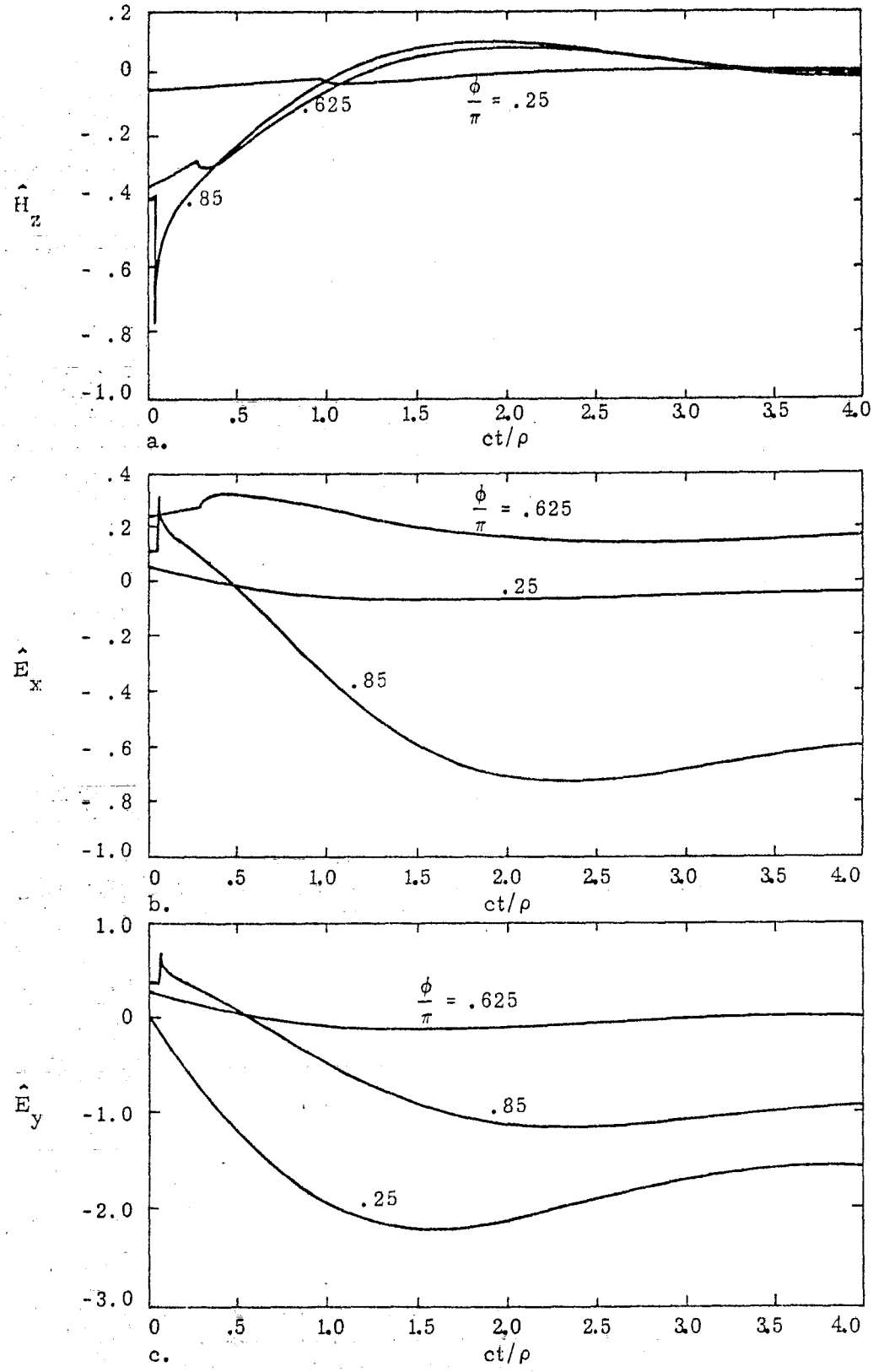

Figure 23. Field Calculation: $\rho = 1.5$, $\alpha = 0.9\pi$

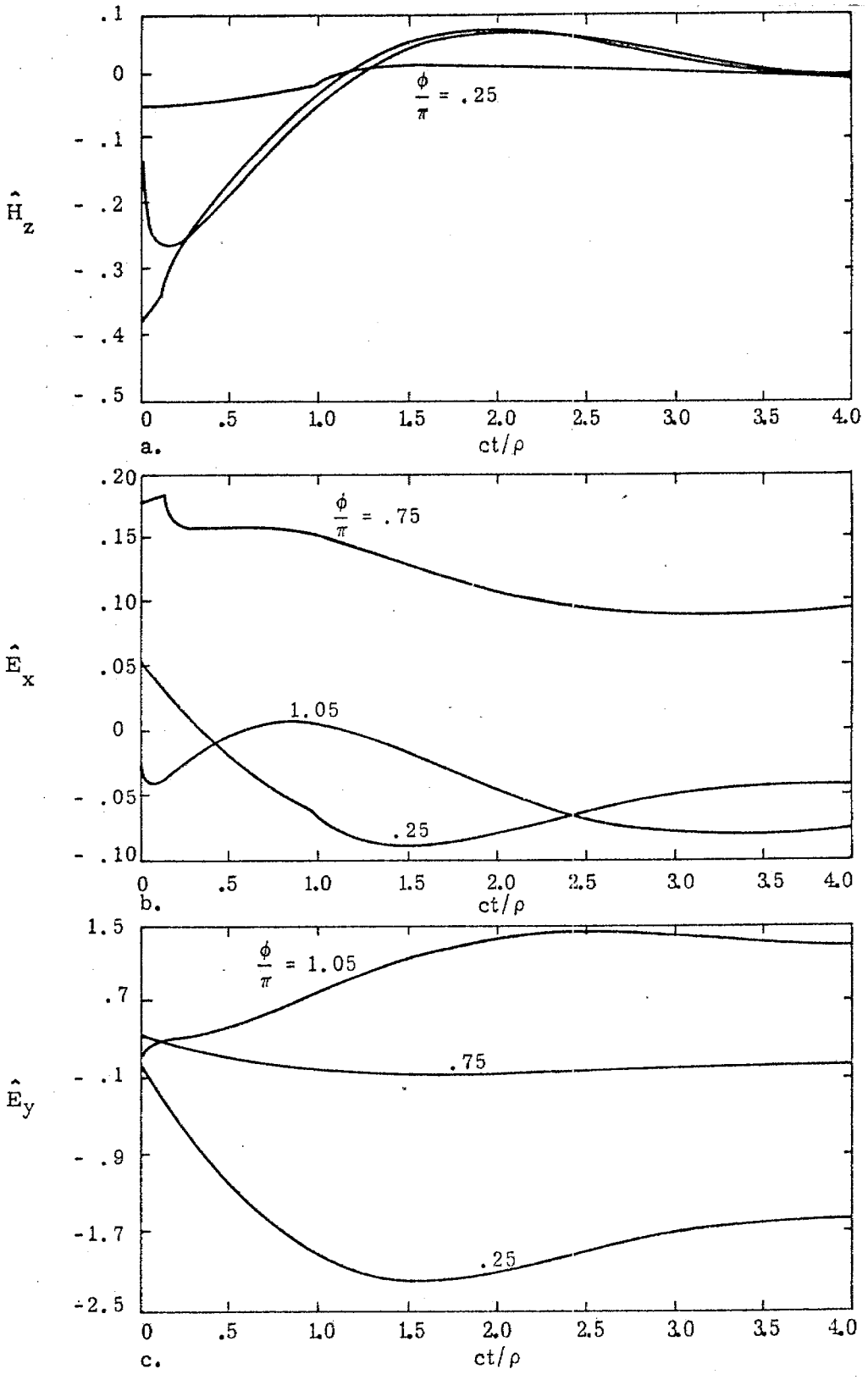

Figure 24. Field Calculation: $\rho = 1.5$, $\alpha = 1.1\pi$

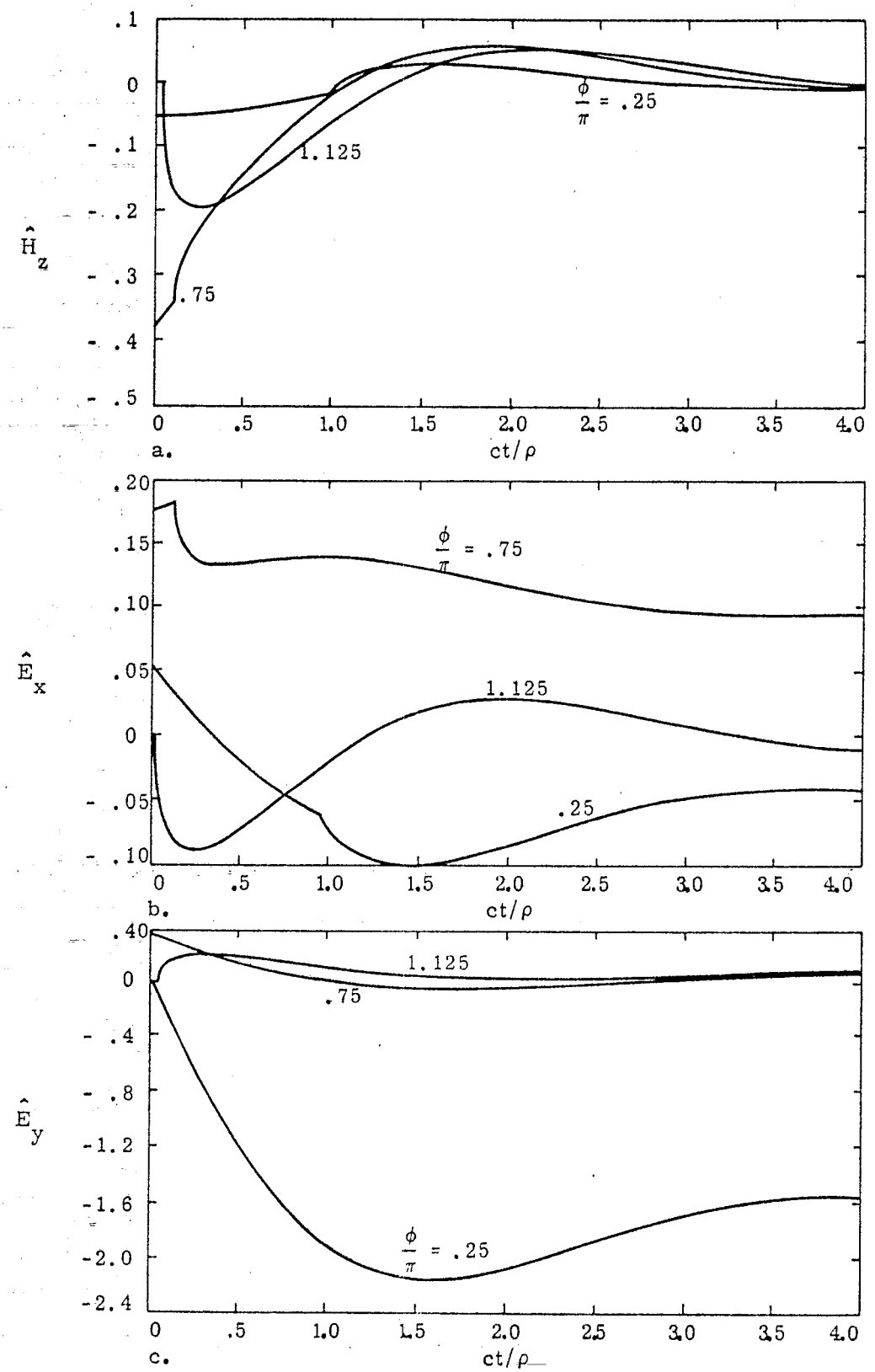

Figure 25. Field Calculation: $\rho = 1.5$, $\alpha = 1.25\pi$

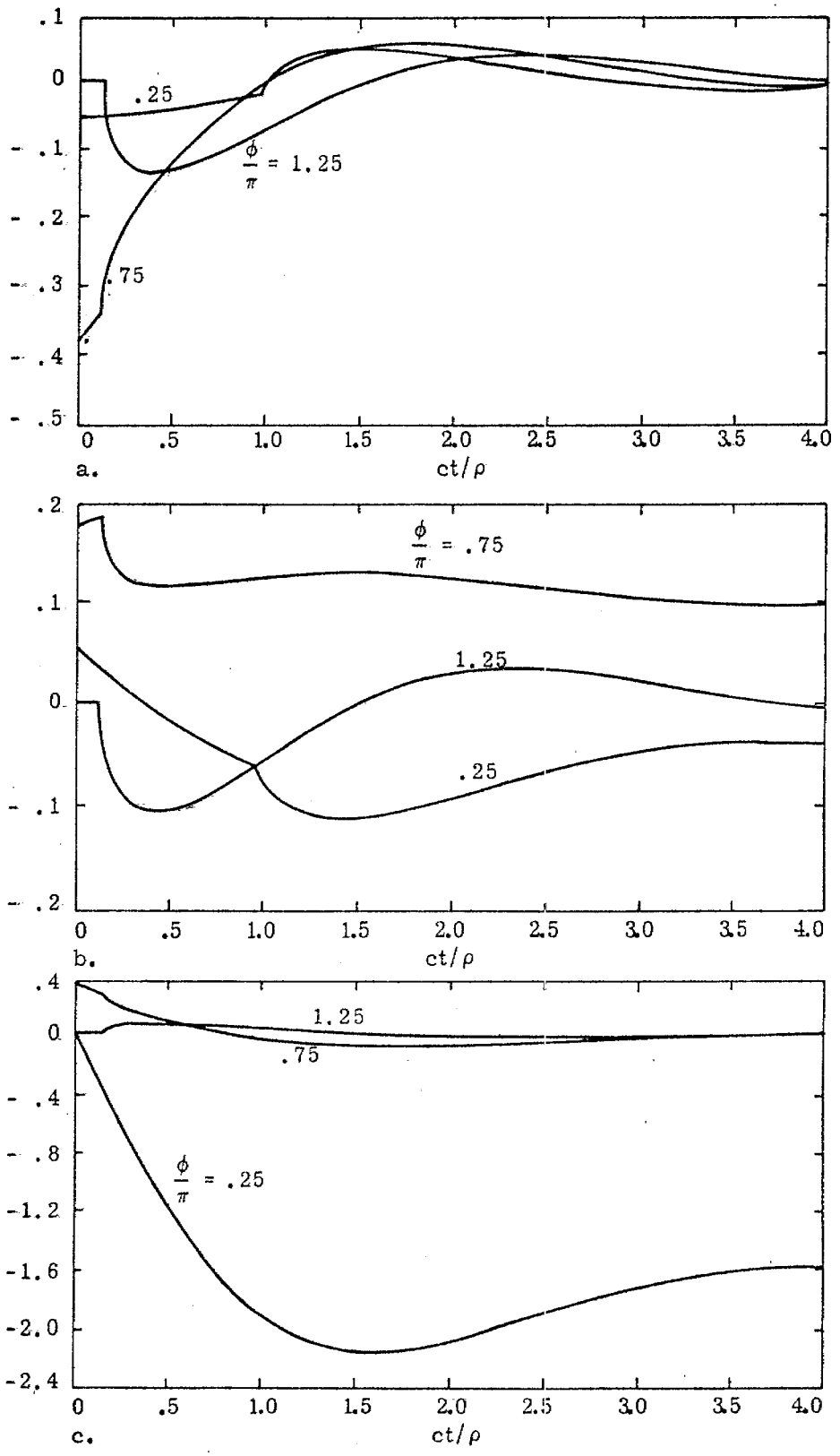

Figure 26. Field Calculation: $\rho = 1.5$, $\alpha = 1.5\pi$